Coral Reefs
https://doi.org/10.1007/s00338-025-02630-z

REPORT

Depth diagnostic mesophotic assemblages in the Northern Red Sea (Saudi Arabia) as analog to the Cenozoic fossil record

Hildegard Westphal[1,2,3,4] · Fabio Marchese[2,5] · Francesca Giovenzana[6] · Guillem Mateu Vicens[7] · Marco Brandano[8] · Valentina A. Bracchi[9] · Silvia Vimercati[2,10] · Volker Vahrenkamp[2,6] · Toshiya Kanamatsu[11] · Alexander Petrovic[2,6,12]

Received: 7 June 2024 / Accepted: 30 January 2025

Abstract While mesophotic assemblages in the Gulf of Aqaba have been described in some detail, in the Red Sea proper, data are rare. Here we present a first report on a detached carbonate platform fragment from the Northern Red Sea off Al Wajh that stretches over a water depth range of 25 to 130 m. The assemblages observed comprise depth-typical large benthic foraminifers, crustose coralline algae, and mesophotic scleractinian corals (e.g., *Leptoseris* spp.). Encrusting bryozoans and foraminifers are abundant. A soft sediment cover in the deeper areas indicates the absence of strong currents. Radiocarbon ages confirm that this community is currently thriving. This example resembles the previously known occurrences of mesophotic reefs in the Gulf of Aqaba with respect to assemblage despite different oceanographic conditions. At the same time, it reminds of Cenozoic, in particular pre-Upper Miocene (i.e., before 8.5 million years ago), coral-associated assemblages, when coral bioherms preferentially occurred in mesophotic rather than euphotic settings. The present study thus contributes to improving the interpretation of those fossil bioherms with respect to their ecosystem dynamics and environmental significance.

Keywords Mesophotic ecosystems · Red Sea · Corals · Large benthic foraminifers · Encrusting foraminifers · Holocene

Supplementary Information The online version contains supplementary material available at https://doi.org/10.1007/s00338-025-02630-z.

✉ Hildegard Westphal
hildegard.westphal@leibniz-zmt.de

[1] Physical Science and Engineering Division, King Abdullah University of Science and Technology (KAUST), Thuwal, Saudi Arabia

[2] Red Sea Research Center (RSRC), King Abdullah University of Science and Technology (KAUST), Thuwal, Saudi Arabia

[3] Leibniz Centre for Tropical Marine Research (ZMT), Bremen, Germany

[4] Department of Geosciences, University of Bremen, Bremen, Germany

[5] Biological and Environmental Science and Engineering Division, King Abdullah University of Science and Technology (KAUST), Thuwal, Saudi Arabia

[6] Ali I. Al-Naimi Petroleum Engineering Research Center (ANPERC), King Abdullah University of Science and Technology (KAUST), Thuwal, Saudi Arabia

[7] Universitat de Les Illes Balears, Palma, Spain

[8] Università La Sapienza, Rome, Italy

[9] CoNISMa Local Research Unit, Department of Earth and Environmental Sciences, University of Milano-Bicocca, Piazza Della Scienza 4, 20126 Milano, MI, Italy

[10] Marine Science Program, Biological and Environmental Science and Engineering Division, King Abdullah University of Science and Technology (KAUST), Thuwal, Saudi Arabia

[11] Research Institute for Marine Geodynamics (IMG), JAMSTEC, Natsushima-Cho 2-15, Yokosuka, Japan

[12] Present Address: CARMEUSE R&D, Louvain-La-Neuve, Belgium

Published online: 12 February 2025

Introduction

Modern mesophotic coral-associated assemblages have received intensive scientific attention in recent years (Slattery et al. 2024). Nevertheless, they are still much less intensively studied than shallow-water coral reefs (Hinderstein et al. 2010). Besides the gaps in understanding the composition and dynamics of those ecosystems, this has biased the interpretation of fossil coral reefs of the Cenozoic toward an interpretation analogous to modern euphotic coral ecosystems with a typical arrangement of a lagoon, a reef fringe, and a steep fore-reef slope. In contrast to that view, however, several studies of fossil coral bioherms have pointed to a predominantly mesophotic nature of those ecosystems thriving as mounds on deeper slopes, prior to the late Miocene, i.e., before 8.5 million years ago (Pomar and Hallock 2007; Pomar et al. 2017). This means that the presence of corals in the geological record in particular before the late Miocene does not necessarily imply a euphotic setting, and applying modern euphotic analogs can lead to misinterpretation (Pomar et al. 2017).

Modern Mesophotic Coral Ecosystems (MCEs) have been described since the 1960s (Busby 1966; Brock and Chamberlain 1968; Strasburg et al. 1968; Goreau and Goreau 1973; Bouchon 1981; Sheppard 1982; Schlichter et al. 1985, 1986, 1994, 1997; Fricke and Meischner 1985; Colin et al. 1986; Fricke and Knauer 1986; Fricke et al. 1987; Thresher and Colin 1986; Schlichter and Fricke 1991; Kaiser et al. 1993; Pyle 2019; Reolid et al. 2024). MCEs are light-dependent tropical and subtropical ecosystems that occur in water depths between ca. 30 m to the lower limit of the photic zone at ca. 150 m; depending on the local conditions, they thrive in shallow settings where low water transparency is limiting light penetration, while in clear and oligotrophic waters they grown at greater water depth, given that oceanographic conditions provide the trophic resources (e.g., Lesser et al. 2009; Hinderstein et al. 2010; Pyle and Copus 2019; Pomar et al. 2017).

The definition of MCEs is not unequivocal, and in the geological record relies on inference from modern mesophotic analogs. A major hindrance in identifying and interpreting fossil MCEs is the scarcity of studies on modern occurrences beyond the classical locales such as the Gulf of Aqaba. While the Red Sea has long been recognized as a hotspot of marine biodiversity and endemism (Briggs and Bowen 2012; DiBattista et al. 2016), as for many other regions of the world, mesophotic waters have not been studied as intensively as the shallower ones, and there is still incomplete knowledge of these environments (Berumen et al. 2013, 2019). In particular, most of the studies of mesophotic organisms in the Red Sea are focused on scleractinian corals of the Eilat coast of the Gulf of Aqaba (see for example Fricke and Hottinger 1983; Fricke and Schuhmacher 1983; Fricke and Knauer 1986; Schlichter et al. 1986; Mass et al. 2007; Stambler et al. 2008; Alamaru et al. 2009; Einbinder et al. 2009; Nir et al. 2011), while few studies address Egyptian and Sudanese waters (Kühlmann 1970; Fricke 1996). There is little information on the mesophotic ecology and the composition of other marine taxa, such as octocorals (Shoham and Benayahu 2017; Eyal et al. 2019), bryozoans (Scholz and Hillmer 1995; Hillmer et al. 1996), and crustose coralline algae (CCA) (Hottinger 1983; Dullo et al. 1990). Recently, some expeditions with a focus on the mesophotic zone were carried out along the Saudi Arabian Red Sea (Ziegler et al. 2015; Purkis et al. 2022; Maggioni et al. 2022; Terraneo et al. 2022, 2023; Bracchi et al. 2023; Anker et al. 2023; Vimercati et al. 2023, 2024a, 2024b; Vicario et al. 2024a, b). However, the geomorphology, the composition, as well as the vertical zonation of the benthic taxa in the mesophotic zone are still only incompletely described or understood, beyond a few studies focusing on the Gulf of Aqaba (Weinstein et al. 2021) or the Central Red Sea (Watts 2022). In particular, mesophotic ecosystems in the Saudi Arabian part of the Northern Red Sea remain still largely unknown.

The present study aims at adding to the knowledge on modern MCEs, and thus to contribute to the identification and discussion of fossil MCEs, by studying an isolated carbonate platform to the south of the land-attached Al Wajh carbonate platform in the Saudi Arabian Northern Red Sea (Fig. 1).

Study area

The Red Sea is a semi-enclosed young ocean basin spreading at a low rate (e.g., Tapponnier et al. 2013; Augustin et al. 2021; Delauny et al., 2023). The continental rifting started during the Oligocene, and first marine flooding is thought to have taken place during the Early Miocene. Restricted conditions during the Mid- to Late Miocene lead to the deposition of an evaporite sequence with a total thickness of up to 2–4 km (Hughes and Johnson 2005). The plastic basinward withdrawal of Miocene salt layers (Heaton et al. 1995; Orszag-Sperber et al. 1998; Rowan 2014) shapes the modern morphology of the Red Sea through collapsing and fragmentation of carbonate platforms, and rafting of the fragments (Petrovic et al. 2023a; Smith and Santamarina 2022). The study area is located south of the land-attached coral reef-rimmed Al Wajh carbonate platform in the Saudi Arabian northern Red Sea (Fig. 1). The western, ocean-facing rim of the Al Wajh platform with a length of around 55 km is likely controlled by its position on the edge of a tilted rift block (Dullo and Montaggioni 1998), while the northern margin is shaped by the Zabargad Fracture Zone (Petrovic et al. 2023b). The southern margin is fragmented as a response to

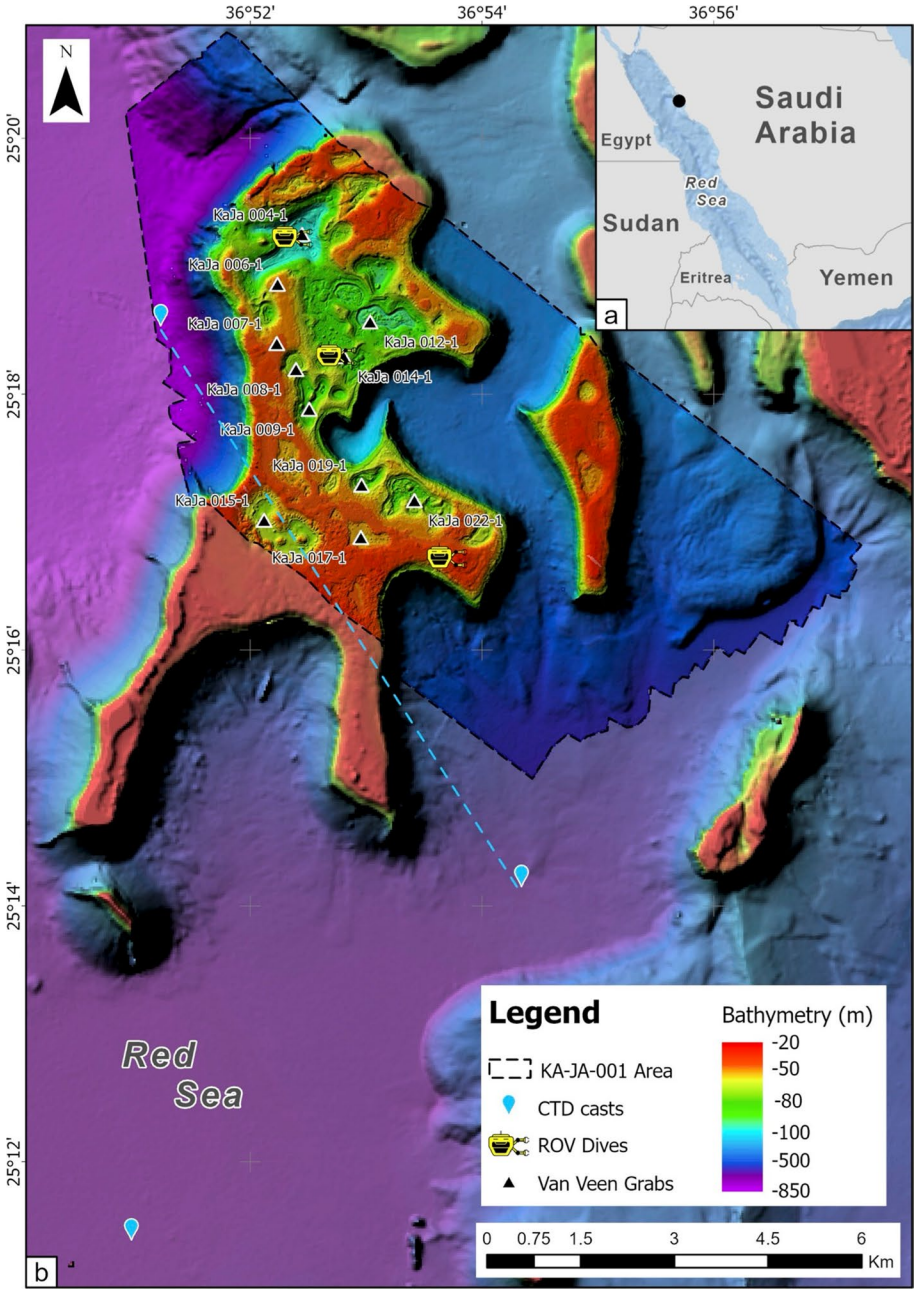

Fig. 1 Location of study area in the Northern Red Sea and close-up of location of studied platform fragment; multibeam bathymetry recorded during RV Thuwal cruise KA-JA-001 cruise, and location of the ROV dives, CTD, and Van Veen grab stations. Also, NW–SE section shown in Fig. 2 is indicated. Basemap from ArcGIS Ocean. Sources: Esri, GEBCO, NOAA, National Geographic, DeLorme, HERE, Geonames.org, and other contributors

basinward salt-withdrawal with the fragments rafting toward the Red Sea axis and being subject to differential subsidence rates (Petrovic et al. 2023a). The study site is one of those isolated carbonate platform fragments (Fig. 1). The fragment has dimensions of 10 km by 4 km in lateral extension (Petrovic et al. 2023a), with its top in water depths ranging from 20 to 130 m.

The prevailing wind direction in the northern Red Sea is northwest, with occasional storms affecting the study area from the south. Intensive jets blowing from the east carrying dust also occur (Petrovic et al. 2023c). In summer, the average water surface temperature ranges from 26˚C in the north to 30˚C in the south. The average water surface winter temperature is around 23 ± 3˚C. Low precipitation (Ø 1–20 cm $y-1$) and high evaporation (ca. 2 m $y-1$; Maillard and Soliman 1986; Siddall et al. 2004) result in sea surface salinities ranging from 36.5 ‰ (S) to 41 ‰ (N). The Red Sea is characterized by an anti-estuarine-like circulation (Sofianos and Johns 2015). During the summer, the water body is subdivided into the Red Sea Surface Water (RSSW: 0–150 m) and the Red Sea Deep Water (RSDW: > 150 m), while during the winter, a third water mass appears, namely the Red Sea Intermediate Water (RSIW: 50–200 m; e.g., Yao et al. 2014). Both, the

RSDW and the RSIW are related to two thermohaline cells (Sofianos and Johns 2015).

Material and methods

The objective of the RV Thuwal cruise KA-JA-001 in February 2022 was to investigate the mesophotic zone south of the Al Wajh carbonate platform from a sedimentological, biological, and oceanographic perspective (Station list see Supplementary Materials S1). Based on an earlier bathymetric data set collected in 2019 (Petrovic et al. 2023a), additional detailed acoustic seafloor data were collected with a Kongsberg EM710-MK2 (40–100 kHz) multibeam echosounder system (MBES), hull-mounted on the RV Thuwal. The bathymetry was used as orientation for the deployment of the instruments and sampling devices during the cruise. The water column was studied with an Idronaut Ocean Seven 310 multiparameter conductivity, temperature, and depth (CTD). Conductivity (salinity calculated), pH, and temperature depth profiles were measured with a sample rate of 200 ms and winch speed of around 0.5 m/s.

Acoustic data have been processed using QPS Qimera software v.2.4.1, sound velocity speed was calculated from the CTD casts at Station 1 and Station 26, and two final gridded bathymetric model were produced: a 20 m grid model of the entire survey area and a fine scale 5 m grid for the shallow platform (25—130 m depth). Geomorphometric analysis and spatial analysis were performed using SAGA GIS v 9.0 (Conrad et al. 2015) and ArcGIS® PRO v 3.1.2. In order to characterize the morphologies of the platform, we used the Geomorphons tool (Jasiewicz et al., 2013) that provided a panoramic view of terrain morphology and highlighted the tridimensional complexity of the area. The complex morphologies of the platform make manual identification and characterization of depressions impractical without extremely time-consuming manual mapping, which can also be subject to operator bias. To identify and characterize the depressions on the platform with a quantitative approach, we used the Geomorphons tool (Jasiewicz et al., 2013) and we follow the nested surface depressions procedure from Wu et al. 2019 using Lidar package for ArcGIS PRO (Wu, 2021). This method combines a boundary-tracking algorithm with graph theory to precisely identify and measure depressions in digital elevation models, categorizing them hierarchically. Once the depressions were identified, we calculate the Shape Index (SI) (McGarical and Marks 1995) values. The SI is a metric used to quantify the complexity of patch shapes, frequently applied in habitat mapping studies to characterize seafloor morphologies (Kendall et al., 2008; Bracchi et al., 2017, Marchese et al. 2020). In the present study, SI was used for polygons representing depressions. It is calculated by comparing the perimeter of each polygon to the perimeter of a perfectly compact, standard shape (e.g., a circle) with the same area, thereby providing insight into the degree of irregularity in the geometry of the depressions.

A visual survey was conducted with the remotely operated vehicle (ROV) of KAUST (SAAB Seaeye Falcon), equipped with an HD 1Cam SubC camera integrated with 62 mm parallel lasers, a Teledyne M series Forward Looking Sonar (FLS) to enhance navigation, obstacle avoidance capabilities, and a Tritech PA500 altimeter. Three ROV mesophotic dives (Fig. 2) were carried out at three different mesophotic depths: 38 m (Station 23, upper mesophotic), 70 m (Station 24, lower mesophotic), and 130 m (Station 25, lower mesophotic). Video footages of each dive were analyzed using VLC Media Player (Videolan 2006). A representative frame grab of each dive was taken in order to describe the benthic assemblages referring to a specific taxon and its distribution. All the data were integrated and analyzed using ArcGIS® PRO v 3.1.2 software by Esri.

A total of 16 seafloor samples were collected (Fig. 1) with a Van Veen grab sampler (1000 cm^2) to characterize the benthic community in the laboratory (biogenic grain identification under the binoculars and by thin section analysis). Grain size analyses were not undertaken, because the potential loss of finer fractions during the process of Van Veen grab sampling could have induced some bias. Foraminifers were identified to species level based on the literature (Hottinger et al. 1993; Loeblich and Tappan, 1994; Al-Dubai et al. 2017), and nomenclature was updated according to WoRMS (2024). Coral identification and nomenclature followed Brook (1889) and Opresko (2001, 2002, 2004) for the order Anthipataria, Gray (1857), Kükenthal (1908) for octocorals, and Veron (2000), Al Tawaha et al. (2019), and Benzoni (2022) for scleractinians.

For six coral and three biogenic carbonate crust samples, ^{14}C AMS ages were determined with accelerator mass spectrometer radiocarbon at the MICADAS AMS facility of Alfred Wegner Institute in Bremerhaven, Germany, following the method described by Mollenhauer et al. (2021). The dates were calibrated with CALIB version 8.2 (Stuiver and Reimer 1993), using the calibration data set Marine20.14c; weighted mean delta R: 15 and uncertainty: 52; based on a coral data set from Ras Umm Sidd (Felis et al. 2004).

Results

Bathymetry and geomorphometric analysis

In total, the bathymetric survey covered an area of 80.5 km^2 (Fig. 1). The resulting bathymetric map includes the isolated carbonate platform that has a serrated shape and reaches maximal dimensions of 10×4 km. Water depths on the platform range from 25 to 130 m water depth

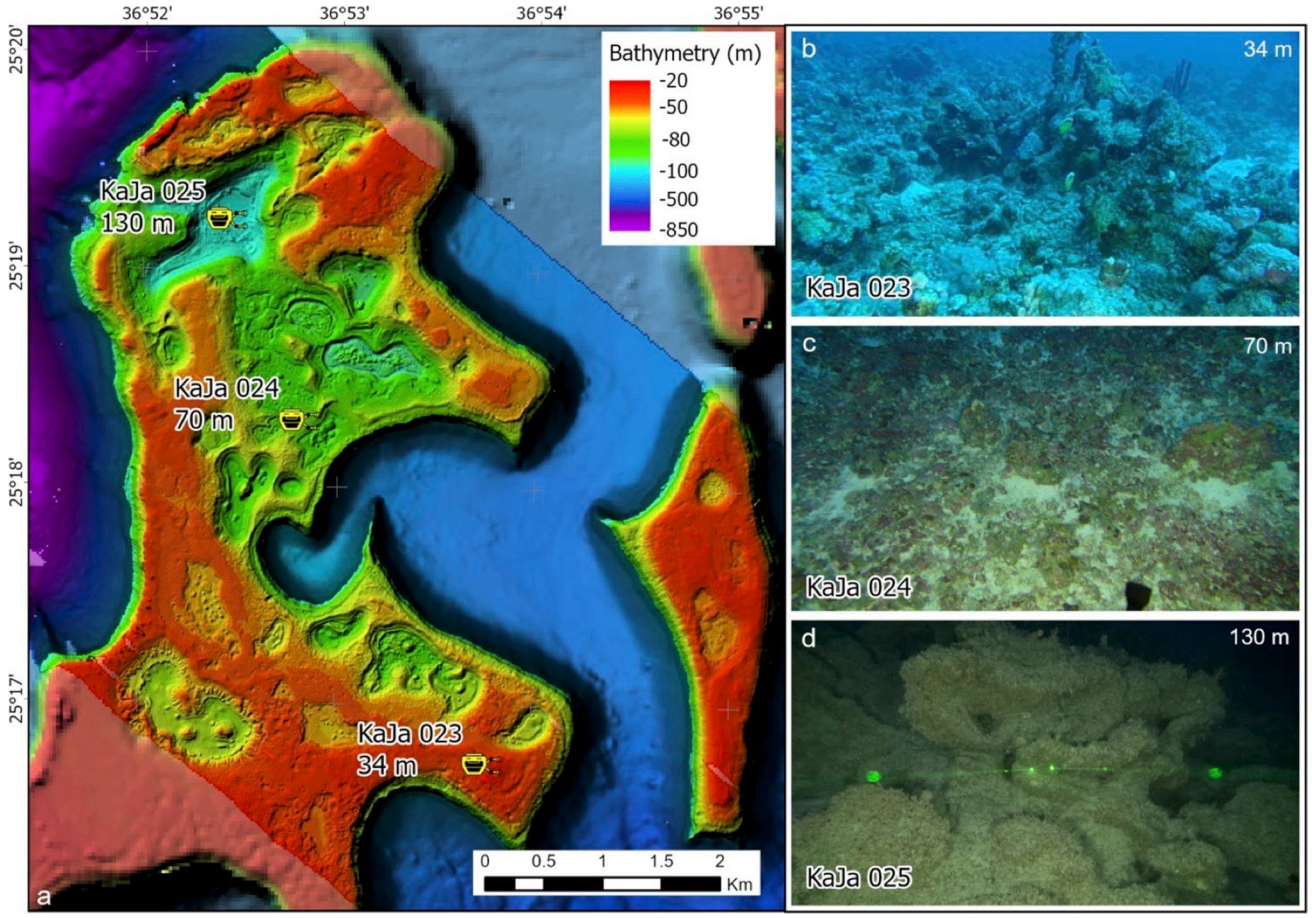

Fig. 2 Location of ROV dives and examples of video frames. The distance of the laser pointers is 6.2 cm.

(mwd). The top of the platform fragment shows a rough morphology including multiple depressions and pinnacles (Fig. 3). It is bordered by steep slopes, up to 83° inclined in the upper parts, toward sediment basins (400–750 mwd). The lower part of the slope facing the basin to the West is characterized by a gradient greater than 30°, while the slope facing the 400 m deep basin to East is mainly defined by a slope gradient exceeding 45°. The fine scale resolution bathymetric grid of the platform was used to perform the geomorphometric analysis to characterize the direction of the depressions and the complex morphology. The result of the geomorphon tool (Jasiewicz et al., 2013) on the platform fragment revealed a rough morphology including multiple depressions and pinnacles (Fig. 3). The nested surface depressions analysis after Wu et al., (2019) identified in 317 depressions, with a depth range from 1 to 56 mwd. For these depressions, for further analysis we selected only those with an SI greater than 1.5, indicating reduced sphericity and a tendency toward elongation. On the resulting pool of 146 depressions (S2), we calculated the maximum diameter bearing and grouped them in four direction classes (S3).

Water profiles

CTD casts were performed at two sites to the NW and SE of the isolated carbonate platform fragment (Stations 1, 26; Fig. 4). At both stations, the sea surface temperature was around 23 °C, while salinity was at the Station 1 (windward) 39.8 PSU and at Station 26 (leeward) 40.05 PSU. Downward depths, salinity rapidly increased to 40.25 PSU until 50 m water depths and further downward gradually increasing until 245 m water depths, identified as the base of the RSSW. Temperature decreased at Station 26 from 23 °C at the surface to 22.2 °C at 245 m, while it stayed constant at Station 1. Between 245 and 250 m water depth (thermocline), the temperature significantly decreased to 26.6 °C at both stations, while salinity increased to 40.6 PSU. Below 250 m water depths showed only minor variations in temperature and salinity in a water body interpreted as the RSDW. The CTD cast clearly showed that the studied area is located within the reach of the RSSW and features an upper mixing zone (0–50 m).

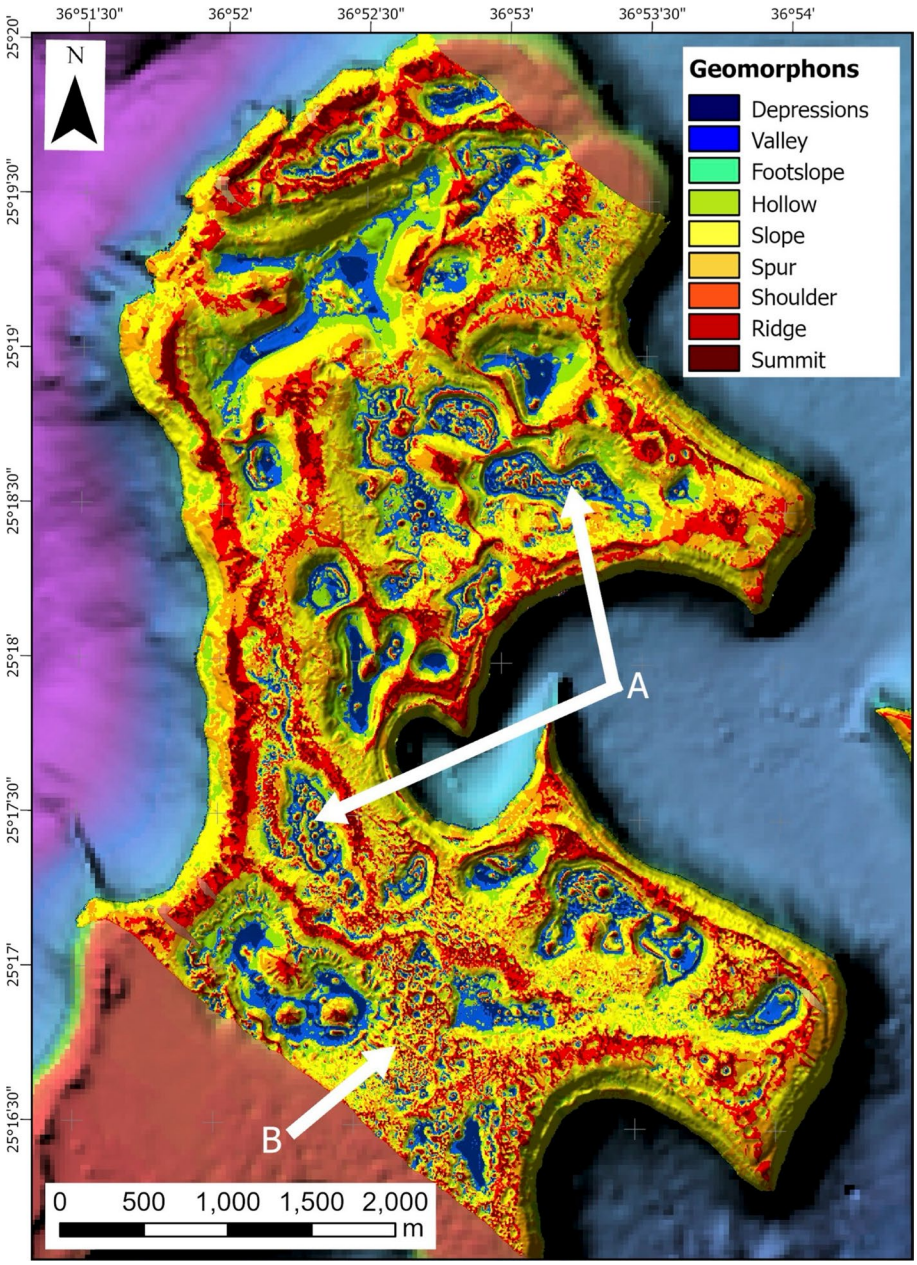

Fig. 3 Geomorphological classification of the survey area using the Geomorphon tool. Color code represents the geomorphic classes calculated by the algorithm: Depressions (Dark Blue), Valleys (Blue), Footslopes (Light Blue-Green), Hollows (Green), Slopes (Yellow), Spurs (Orange), Shoulders (Light Red), Ridges (Red), Summits (Dark Red). The high resolution of the model combined with the result of the tool reveal abundant small pinnacles (A) and reticular structures (B) that are interpreted as expression of biological activities (buildups)

Benthic assemblages

For the three stations where ROV footages were recorded (transition from deep euphotic to shallow mesophotic: 25–38 m, Station 23; deep mesophotic: 74 m, Station 24; transition from deep mesophotic to aphotic: 130 m, Station 25), the benthic assemblages were characterized visually. On those ROV-obtained frame grabs (Fig. 2), the following organism groups were identified: crustose coralline algae (CCA), encrusting foraminifera, sponges, bryozoans, black corals in the Order Antipatharia Milne Edwards, 1857, octocorals, and four scleractinian families, namely Agariciidae Gray, 1847, Poritidae Gray, 1840, Merulinidae Milne Edwards and Haime, 1857, and Dendrophylliidae Gray, 1847 (Table 1).

At Station 23 (25–38 m water depth), ROV footage revealed abundant Poritidae as well as abundant encrustation by CCA and foraminifera on a morphology with decimeter to meter scale bulbs. Other live organisms included sponges, octocorals, soft corals, Agariciidae and Merulinidae, and rare Antipatharia. At Station 24 (74 m water depth), encrustations prevailed; however, less CCA were identified. Generally, there was abundant fine-grained sediment covering part of the seafloor. Agariciidae were present as the most abundant corals, while Poritidae and Merulinidae were not identified. Antipatharians were more abundant than in the

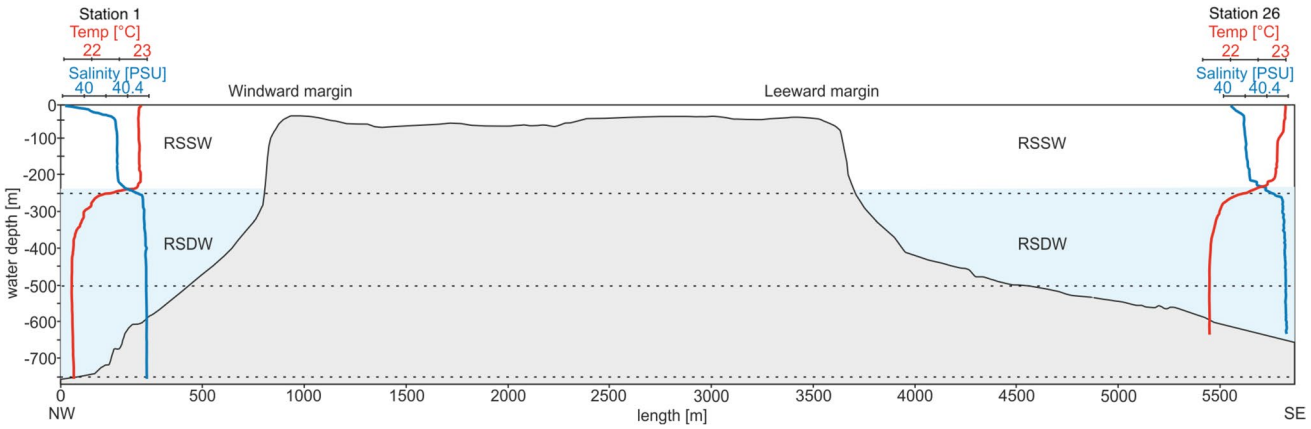

Fig. 4 NW–SE topographical cross section, including water masses and CTD temperature and salinity profiles. Station 1 is located at the windward margin, while Station 26 is located at the leeward margin (see Fig. 1). Temperature and salinity profile define the water mass boundary on the windward and leeward side of the platform in the same water depths. RSSW: Red Sea Surface Water, RSDW: Red Sea Deep Water. Vertical exaggeration is × 1.2

Table 1 Benthic taxa recorded on ROV footage. x = rare, xx = common, xxx = abundant

Station	23	24	25
Water depth	38 m	70 m	130 m
CCA	xxx	xxx	x
Antipatharia Milne Edwards, 1857	x	xx	xxx
Octocorals	xx	xx	xxx
Agariciidae Gray, 1847	xx	xxx	
Poritidae Gray, 1840	xxx		
Merulinidae Milne Edwards, 1857	xx		
Dendrophylliidae Gray, 1847	x	xx	xxx

shallower station. The seafloor morphology was flatter than in the shallower setting; however, it was still dominated by biological buildups. At Station 25 (130 m water depth), CCA were rare, and more common Antipatharia and Dendrophylliidae corals represented the coral diversity. A cover of abundant fine-grained sediment pointed to low water energy.

Sediment composition of lithified and encrusted samples

A total of 16 Van Veen grab samples were taken from water depths between 27 and 120 m. Recovery was very variable depending on the seafloor conditions, where medium to fine-grained sediment allowed for very good recovery, while hardgrounds (biogenically encrusted seafloor) and bulbous morphology led to variable and partly very poor recovery. Two stations had to be discarded because of low recovery.

The samples featuring encrustations and bioherms showed the following characteristics: At the shallowest site, Station 18 (25 m), a dead coral colony was sampled, consisting of coral skeleton colonized by other biota, including CCA. At 47 m (Station 7), CCA crusts and fine-grained sediment were accompanied by fleshy green algae, indicating (deep) euphotic conditions. At 57 m water depth (Station 17), CCA-covered rubble-sized grains and fine-grained sediment were recovered. Sediment from Stations 5 (27 m), 13 (46 m), and 21 (60 m) showed CCA crusts without any accompanying fine-grained sediment. Stations 16 (42 m), 14 (74 m), and 22 (77 m) feature CCA crusts and some fine-grained sediment. At 82 m (Station 19), the recovered sediment consisted of CCA-covered rubble-sized grains.

Thin sections were prepared from seven samples collected at stations where the grab recovered solid biogenic substrates (Fig. 5; Table 2). The most common components identified were encrusting foraminifers and scleractinian corals. Encrusting foraminifers were present in samples from Stations 14 (74 m) and 19 (82 m), dominated by Acervulinidae Schultze, 1854, but also including *Homotrema rubrum* (Lamarck, 1816). Corals occurred as rubble (Station 17, 57 m), solitary corals, and colony fragments (Stations 5, 14, 16, 18, and 19, between 25 and 82 m) (Table 2). While Poritidae were identified in samples from 27–57 m water depth (Stations 5, 16 and 17), Agaricidae, with a typical platy arrangement, occurred in the entire depth range from 25 to 82 m (Stations 5, 14, 18, 19, and 21) (Table 2). Furthermore, thin CCA crusts were observed in thin sections from Stations 5 and 18, which correspond to the shallowest stations. No diagnostic features that would have allowed for taxonomic determination were identified in the CCA. Rare bryozoans also occur (Station 17, 57 m and Station 21, 60 m). The samples from 57 m water depth (Station 17) included abundant benthic foraminifers, entrapped within the skeletal layers.

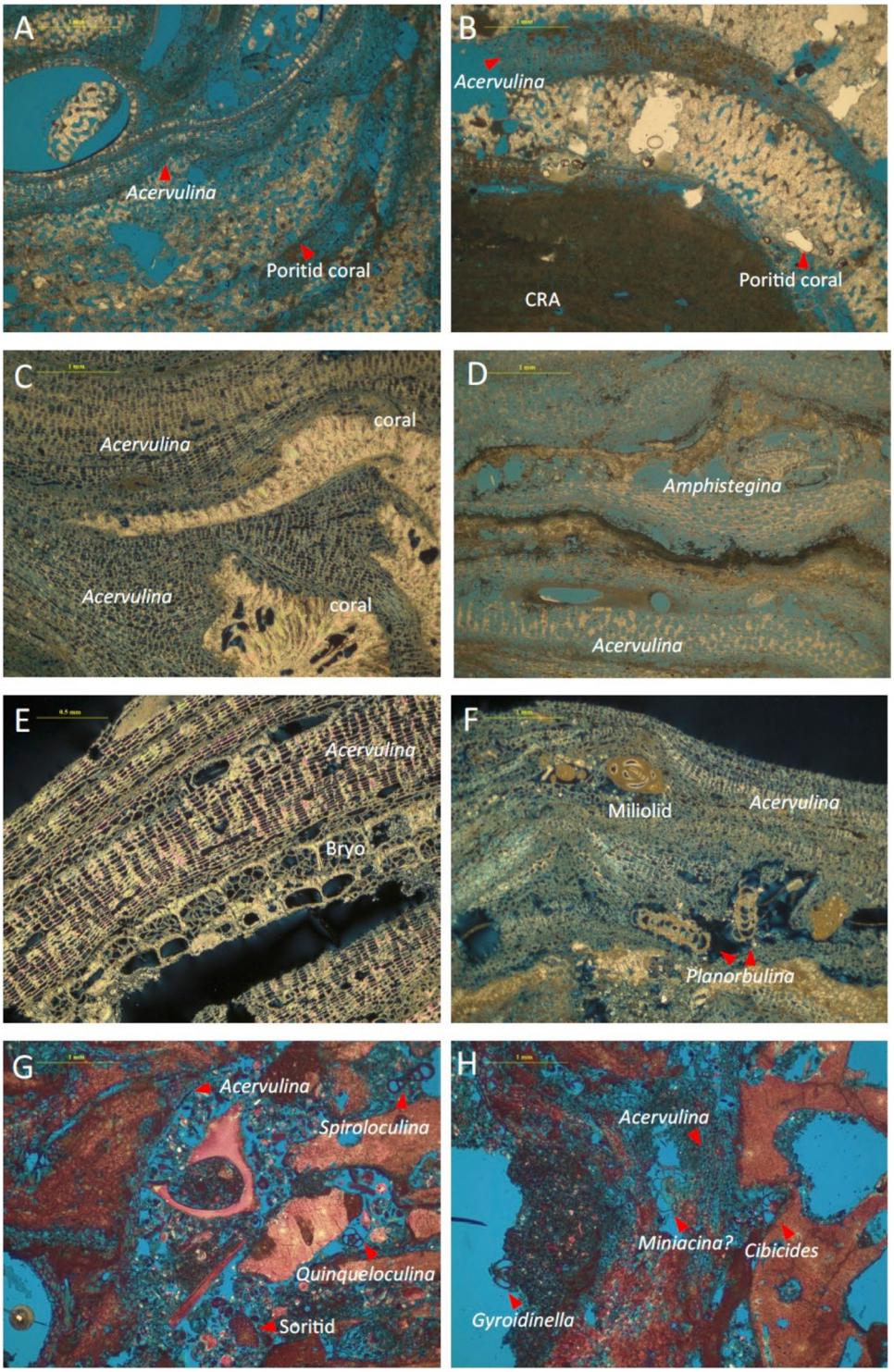

Fig. 5 Thin sections of lithified and encrusted samples (**A**–**C**) interlayered encrusting foraminifers and corals (**A**, **B**: Station 5, C. Station 19), (**D**) interlayered crusts of encrusting foraminifers and crustose coralline algae (Station 19), (**E**) interlayered crusts of encrusting foraminifers and bryozoans (Bryo) (Station 21), (**F**–**H**) encrusting with entrapped benthic foraminifers (**F**: Station 17, **G**,**H**: Station 5). All samples are embedded in blue resin glue; red color in (G, H) is Alizarin-Red stain. (**E**, **F**): crossed nicols

As the samples were taken with a grab, they were not oriented with respect to the vertical sedimentary column. However, for some of the thin sections, it is possible to determine an orientation and order of succession of encrusting organisms. For example, the thin section from Station 5 comprised a fragment of a Poritidae at the base, overgrown by a thin CCA crust, followed by a thick layer of encrusting foraminifers, with an Agariciidae layer within. A thin section from Station 17 showed two solitary corals, with the calyx filled by biogenic mud, and with a thick concentric envelop made by encrusting foraminifers. Thin sections from Station 17 (57 m) included a coral rubble enveloped by a thick layer of encrusting foraminifers.

Table 2 Thin sections. Note: Station 14 corresponds to Dive Station 24; and Station 18 to Dive Station 23

Station	Water depth	Description
5	27 m	Encrusting foraminifers (*Acervulina* spp. Schultze, 1854, *Planorbulina* spp. d'Orbigny, 1826, *Miniacina* spp. Galloway, 1933, *Discanomalina* spp. Asano, 1951), epiphytic foraminifers (*Sorites* spp. Ehrenberg, 1839/*Amphisorus* spp. Ehrenberg, 1839, *Quinqueloculina* spp. d'Orbigny, 1826, *Spiroloculina* spp. d'Orbigny, 1826, *Cibicides* spp. Montfort, 1808), planktic foraminifers (Globigerinidae Carpenter et al., 1862), coral (Poritidae Gray, 1840)
14	74 m	Encrusting foraminifers (*Homotrema* spp. Hickson, 1911, *Acervulina* spp. Schultze, 1854, Victoriellidae Chapman and Crespin, 1930), Large benthic foraminifers (*Amphistegina* spp. d'Orbigny, 1826, *Heterostegina* spp. d'Orbigny, 1826), agglutinated foraminifers (*Trochammina* spp. Parker and Jones, 1859), coral (Agariciidae Gray, 1847), crustose coralline algae (CCA)
16	42 m	Encrusting foraminifers (*Haddonia* spp. Chapman, 1898), planktic foraminifers (*Globigerinoides ruber* [d'Orbigny, 1839]), epiphytic foraminifers (*Peneroplis* spp. Montfort, 1808), coral (Poritidae Gray, 1840)
17	57 m	Encrusting foraminifers (*Acervulina* spp. Schultze, 1854, *Acervulina mabahethi* (Said, 1949), Homotrematidae Cushman, 1927, *Haddonia* spp. Chapman, 1898), small benthic foramnifers (Buliminidae Jones, 1875), coral rubble, solitary corals, serpulids, biogenic mud
18	25 m	Coral (Agariciidae Gray, 1847), encrusting foraminifers (Homotrematidae [Cushman, 1927], *Acervulina* spp. [Schultze, 1854], *Haddonia* spp. [Chapman, 1898])
19	82 m	Encrusting foraminifers (*Acervulina* spp. Schultze, 1854), large benthic foraminifers (*Amphistegina* spp. d'Orbigny, 1826), small benthic foraminifers (Hauerinidae Schwager, 1876, Buliminidae Jones, 1875/ Bolivinitidae Cushman, 1927, Nodosariidae Ehrenberg, 1838, *Nonion* spp. Montfort, 1808), planktic foraminifers (Globigerinidae Carpenter et al., 1862), corals (Agariciidae Gray, 1847)
21	60 m	Encrusting foraminifers (*Acervulina* spp. Schultze, 1854, *Planorbulina* spp. d'Orbigny, 1826), corals (Agariciidae Gray, 1847), coral rubble

Fine-grained unconsolidated sediments recovered showed the following characteristics: At 65 m water depth, a station featuring a fine sediment cover (Station 15), the sediment is moderately sorted and fine-grained; at 69 m (Station 12) and at 73 m (Station 8), sediments are moderately to well-sorted fine-grained sands with abundant small foraminifers. The sediment recovered at 82 m (Station 6) is similar but with less foraminifers. At 87 m (Station 9), moderately to well-sorted fine-sandy sediment was encountered, containing larger benthic foraminifers. At 120 m (Station 4), the recovered fine-grained sandy sediment was well sorted.

Benthic foraminifers from lose sediment samples

A total of eleven sediment samples were analyzed for their benthic foraminifer assemblages (Fig. 6, Fig. 7). At least 250 tests were picked from the > 125 µm fraction. Taxonomic identification was performed at family level, and only groups with a relative abundance above 4% in at least one sample were considered (Table 3). The most abundant families in all samples were Hauerinidae Schwager, 1876 (relative abundance up to 29%), Amphisteginidae Cushman, 1927 (relative abundance up to 44%), and Nummulitidae Blainville, 1827 (relative abundance up to 25.7%). The only exception occurred in a sample from Station 4 (130 m), in which the most abundant families were Bolivinitidae Cushman, 1927 (18.0%), and Cibicididae Cushman, 1927 (28.7%), whereas the three aforementioned families displayed a low relative abundance. Hauerinidae, also referred to as miliolids, have a high abundance (between 15.7 and 29.0%) in samples from Stations 7 (46 m), 8 (73 m), 14 (74 m), 15 (65 m), and 17 (57 m). Two other miliolid families were found to be relevant contributors to the assemblages, namely Alveolinidae Ehrenberg, 1839, and Soritidae Ehrenberg, 1839. With 10.4%, these two families displayed the highest relative abundance in Station 17 (57 m), while both sum up to 7.9% to the total assemblage at Station 7 (46 m) and 9.2% at Station 14 (74 m). With 9.2%, the Alveolinidae family displayed the highest relative abundance in Station 17 (57 m;), while the Soritidae significantly contributes to the assemblages at Stations 7 (46 m) and 14 (74 m), with values, respectively, of 3.1% and 4.4%. Notably these two families are extremely rare or absent at all deeper stations (Stations 4 [130 m], 6 [83 m], 8 [73 m], 9 [86 m], 12 [93 m], 19 [82 m], and 22 [77 m]). Nummulitidae, represented mainly by the species *Operculina ammonoides* (Gronovius, 1781), displayed high percentages (between 17.2 and 25.7%) in samples from Stations 8 (73 m), 9 (86 m), 17 (57 m), 19 (82 m), and 22 (77 m). The family Amphisteginidae, represented by the Genus *Amphistegina* d'Orbigny, 1826, displayed high abundance (between 16.5 and 44.3%) in most of the samples, namely Stations 6 (83 m), 7 (46 m), 9 (86 m), 12 (93 m), 14 (74 m), 17 (57 m), 19 (82 m). Moreover, three families of typically epiphytic foraminifers were found in most samples with variable relative abundances, *i.e.*, Discorbinellidae Sigal, 1952 (maximum relative abundance of 6.6% at Station 4), Rosalinidae Reiss, 1963 (maximum relative abundance of 4.5 at Station 22), and Reussellidae Cushman, 1933 (maximum relative abundance of 5.1% at Station 22). Lastly, the only family of the agglutinated foraminifer group

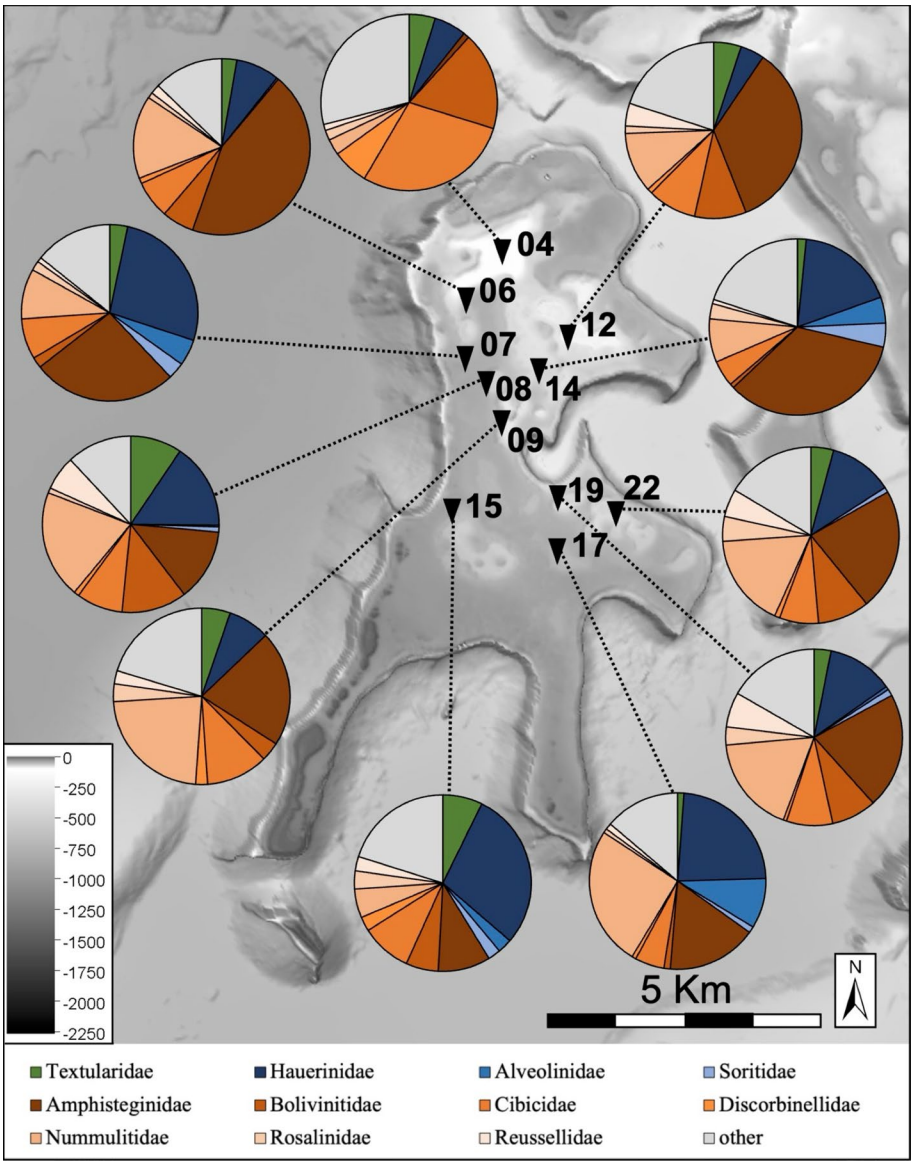

Fig. 6 Location of samples where benthic foraminifer assemblages were determined. The relative abundances of the foraminifer groups are shown in pie charts represent the percentage of different benthic foraminifera families

present was Textulariidae Ehrenberg, 1839, which displayed the highest relative abundances at Stations 8 (73 m) and 15 (65 m), respectively, 9.4 and 7.3%.

Age dating

The results of the radiocarbon dating point to a recent origin of the surface samples (biogenic carbonate crusts and corals, < 700 cal a BP) indicating a formation under very similar conditions as today (Table 4).

Discussion

The geomorphometric analysis undertaken here revealed that the fragment has shallow margins with deeper basins in the northeast. The direction of the main axes of the depressions is mainly E-W and NW–SE, which aligns with the listric faults described by Petrovic et al. (2023a) in the same area. The morphology of the platform (Fig. 3) displays a distinct and complex three-dimensional pattern, characterized by crests, pinnacles, and depressions. The geomorphometric features indicate an environment dominated by positive structures (such as summits, ridges, and shoulders) that not only occur on the top of the platform, but also contribute to the creation of complex morphologies within negative structures (e.g., depressions and valleys) (marked with A in Fig. 3) and along the rims of larger depressions. The southern sector is particularly notable for its reticulated structures (marked with B in Fig. 3) that occur within a depth range of 40 to 55 mwd. Similar reticulated structures have previously been interpreted as biological self-organization (Schlager

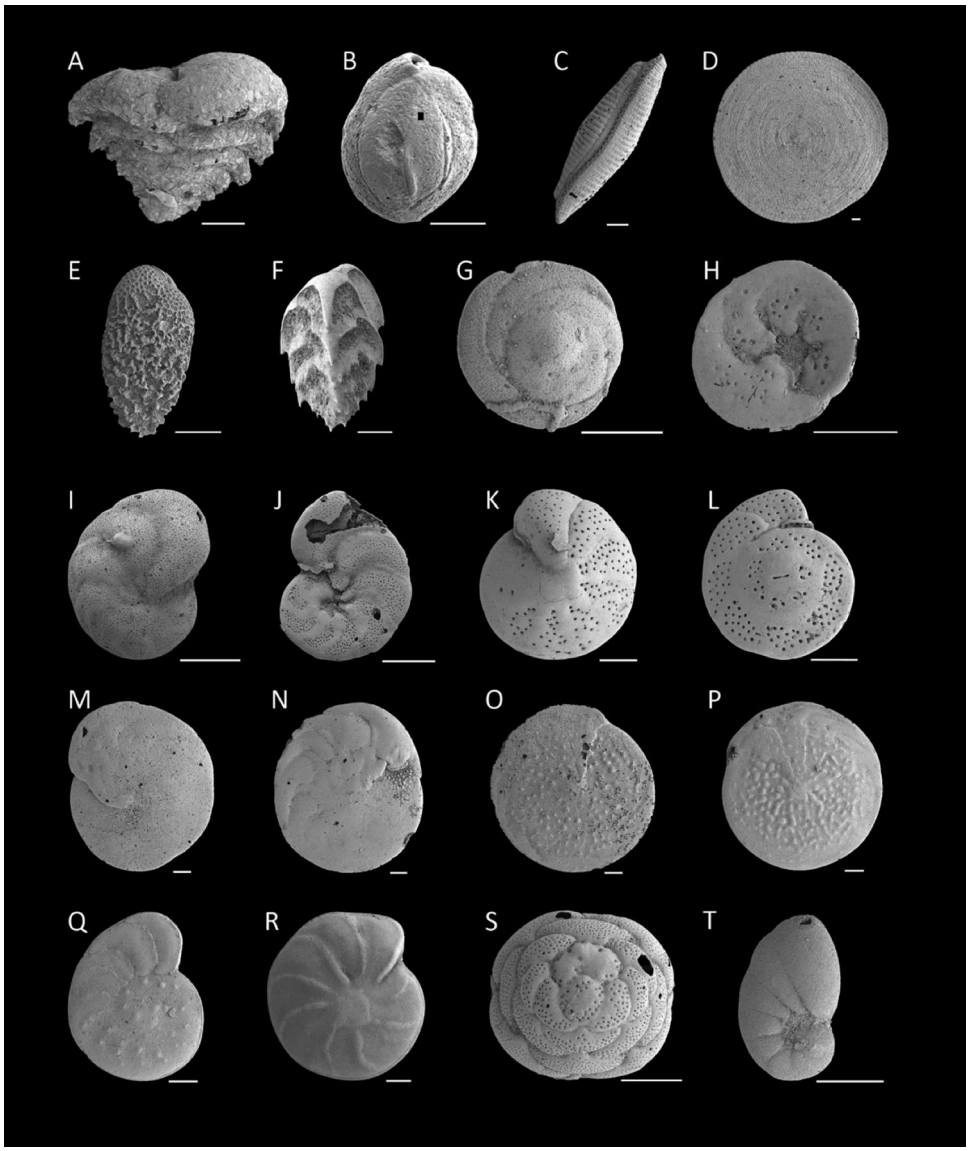

Fig. 7 SEM images of selected Benthic foraminifera species. **A**. *Sahulia kerimbaensis* (Said, 1949), family Textulariidae; **B**. *Pseudoschlumbergerina ovata* (Sidebottom, 1904), family Hauerinidae; **C**. *Borelis schlumbergeri* (Reichel, 1937), family Alveolinidae; **D**. *Sorites orbiculus* (Forsskål in Niebuhr, 1775), family Soritidae; **E**. *Bolivina persiensis* Lutze, 1974, family Bolivinitidae; **F**. *Reussella spinulosa* (Reuss, 1850), family Reussellidae; **G**. *Neoconorbina terquemi* (Rzehak, 1888), family Rosalinidae, spiral side; **H**. *N. terquemi*, umbilical side; **I**. *Hanzawaia boueana*, (d'Orbigny, 1846), family Discorbinellidae, spiral side; **J**. *H. boueana*, umbilical side; **K**. *Heterolepa dutemplei*, (d'Orbigny, 1846), family Cibicididae, spiral side; **L**. *H. dutemplei*, umbilical side; **M**. *Amphistegina bicirculata* Larsen, 1976, family Amphisteginidae, spiral side; **N**. *A. bicirculata*, umbilical side; **O**. *Amphistegina radiata* (Fichtel and Moll, 1798), family Amphisteginidae, spiral side; **P**. *A. radiata*, umbilical side; **Q**. *Operculina ammonoides* (Gronovius, 1781), family Nummulitidae, evolute morphotype; **R**. *O. ammonoides*, involute morphotype; S. *Tretomphalus bulloides* (d'Orbigny, 1839), family Rosalinidae; **T**. *Nonion subturgidum* (Cushman, 1924), family Nonionidae. Scale bars = 100 µm

and Purkis 2015; Xi et al. 2024). These high topographic complexity is in accordance with a constructive role of a living biotic community capable of forming buildup structures as ecosystem engineers.

The present study on the isolated platform fragment off Al Wajh is a first description of a euphotic–mesophotic trend in a coral ecosystem in the Red Sea proper. The shallow part in the South of the platform fragment is characterized by a thriving deep-euphotic coral bioherm characterized by the presence of Poritidae and Merulinidae. The basins in the northern part are submerged in the mesophotic zone, reaching down to 80 m water depth, with deeper depressions of 130 m water depth, featuring abundant Antipatharia, octocorals, and Dendrophyliidae. The benthic community and sediment composition (taxonomic spectrum of corals, benthic foraminifers) represent a succession consistent with a

Table 3 Relative abundance (percentage) of major benthic foraminifer families in sediment samples

Station	Water depth	Textulariidae Ehrenberg, 1838	Hauerinidae Schwager, 1876	Alveolinidae Ehrenberg, 1839	Soritidae Ehrenberg, 1839	Amphistegi-nidae Cush-man, 1927	Bolivinitidae Cushman, 1927	Cibicididae Cushman, 1927	Discorbinel-lidae Sigal, 1952	Num-mulitidae Blainville, 1827	Rosalinidae (Reiss, 1963	Reussellidae Cushman, 1933	others
4	130 m	4.78	5.88	0.00	0.00	1.10	18.01	28.68	6.62	2.94	1.84	1.10	29.04
6	83 m	2.77	7.96	0.35	0.00	44.29	5.88	6.92	1.04	15.22	1.04	1.73	12.80
7	46 m	3.29	26.75	4.82	3.07	26.54	1.97	7.46	0.00	9.21	1.75	0.88	14.25
8	73 m	9.43	15.72	0.31	0.94	13.21	11.95	8.49	0.94	19.81	0.94	6.29	11.95
9	86 m	5.24	7.64	0.00	0.00	21.18	3.49	11.35	2.18	22.93	3.28	2.40	20.31
12	93 m	5.07	4.38	0.00	0.00	34.56	9.45	8.99	0.92	11.06	1.38	4.15	20.05
14	74 m	1.59	17.93	4.78	4.38	34.26	0.80	4.78	0.00	7.97	2.79	0.80	19.92
15	65 m	7.26	29.04	2.64	2.31	9.57	5.94	9.24	2.64	5.28	3.30	2.64	20.13
17	57 m	1.15	23.37	9.20	1.15	16.48	1.15	5.36	0.77	25.67	0.77	1.15	13.79
19	82 m	3.09	12.16	0.62	1.24	21.24	8.25	8.45	0.62	17.94	3.30	6.39	16.70
22	77 m	4.16	11.72	0.00	0.95	22.31	9.45	7.18	0.95	17.20	4.54	5.10	16.45

gradient from deep euphotic to deep mesophotic conditions. The photic trend is clearly reflected in the changes in the benthic taxa, in particular in the benthic foraminifer association. The most indicative group in this study is the large rotaliids, which host diatom symbionts, is represented by the families Amphisteginidae and Nummulitidae. They are very abundant throughout the entire analyzed bathymetric gradient, being very common down to 90 mwd and extremely rare at 130 mwd. The taxa that make up this group may live in euphotic conditions, but their morphological plasticity and the light range that their diatom symbionts can utilize allow their habitats to extend into mesophotic and even oligophotic conditions, particularly in the case of Nummulitidae (Pomar et al. 2017).

Notably, large symbiont-bearing miliolids (Soritidae and Alveolinidae), which are thriving in euphotic environments such as seagrass meadows (Pomar et al. 2017), have been commonly observed in the shallower samples, and become increasingly scarce with increasing depth, eventually disappearing entirely around 85 mwd. The bathymetric range in which they appear, down to 83 mwd, does not correspond to the depth of the habitats they occupy. Therefore, it is highly likely that these large miliolids have been transported from adjacent shallow areas. Among the small benthic foraminifera, the presence of Cibicididae, Discorbinellidae, Rosalinidae, and Hauerinidae, although not exclusive to these habitats, is consistent with the presence of seagrass meadows mentioned earlier, due to the frequently epiphytic nature of many species belonging to these families (Langer, 1993; Mateu-Vicens et al. 2014; Mariani et al., 2022).

Encrustations, dominated by encrusting foraminifers which were the most abundant group in all thin sections, with sporadic CCA and bryozoans, do not show a clear depth trend. This observation of abundant encrusting foraminifers, in particular acervulinids, acting as bioengineers in the mesophotic zone is in line with previous descriptions from the Gulf of Aqaba and the northern Red Sea (Hottinger 1983; Dullo et al. 1990; Bracchi et al. 2023). However, encrustations by corals seem to be restricted to the euphotic zone.

The coral succession observed in the deeper-water depressions of the platform is similar to the mesophotic coral reefs of in the Gulf of Aqaba off Eilat with an upper mesophotic zone (30–80 m) characterized by a high diversity of depth-generalist coral species and a lower mesophotic zone (80–160 m) dominated by the depth-specialist coral *Leptoseris* cf. *striatus* Saville Kent, 1871 (previously referred to as *Leptoseris fragilis* Milne Edwards and Haime, 1849, but also see Benzoni 2022, Vimercati et al. 2024a). The presence of fine-grained poorly sorted sediment covering the deeper parts of the platform fragment conforms with the notion of a near-absence of deep currents along the Red Sea margins (Petrovic et al. 2023b), while deeper-water currents might be present in the central basin of the Red Sea (Zhai et al. 2015).

Table 4 AMS radiocarbon dates and calibrated ages of corals and biogenic crusts

Station	Lab code [AWI]	Material	14C age (a BP)	1σ range (cal a BP)	2σ range (cal a BP)	Median probability (cal a BP)
10	12,547.1.1	A (coral)	− 194 ± 22	x	X	Recent
14	12,548.1.1	A (coral)	446 ± 22	x	X	Recent
14	12,548.2.2	B (crust)	616 ± 22	X	x	603
17	12,549.1.1	A (coral)	1.311 ± 23	770–617	856–538	690
17	12,549.2.1	B (crust)	3 ± 22	x	X	Recent
17	12,550.1.1	A (coral)	687 ± 22	218–41	274–0	134
19	12,551.1.1	A (coral)	577 ± 22	X	x	Recent
21	12,552.1.1	A (coral)	− 459 ± 22	X	X	Recent
21	12,552.2.1	B (crust)	− 367 ± 22	x	X	Recent

Radiocarbon laboratory code: AWI: Alfred Wegener Institute (Germany)

In the present study, sampling was restricted to seafloor surfaces; thus, determination of biotic trends over time as well as a of ages below the upper crusts were not possible, limiting the study to a description of the status quo rather than allowing for a study of the development through time. The observations do not unequivocally substantiate whether the morphology and depth zones observed on this carbonate platform fragment represent an event of drowning in the act caused by extensional faulting or by salt tectonically triggered sliding of the platform fragments (Petrovic et al. 2023a), or whether stable photic conditions were sustained along on the isolated platform fragment for substantial time. The morphology of the platform surface reminds of a palimpsest (i.e., superimposed) morphology resembling a shallow-water reef surface (Fig. 3), which could indicate that the current mesophotic conditions represent a drowning sequence. However, this remains speculation on the basis of the available data.

In many respects, including organism groups and morphological characteristics, the modern mesophotic coral ecosystem described here shows remarkable similarities with fossil assemblages from coral-dominated carbonate factories during the Cenozoic (i.e., during the last 66 million years) (see extensive review by Pomar et al. 2017). This is particularly the case for those coral ecosystems thriving prior to the Upper Miocene (prior to the late Tortonian, i.e., 8.5 million years ago [Ma]) (Pomar and Hallock 2007; Pomar et al. 2017). Prelate-Tortonian bioconstructions in the mesophotic zone were primarily formed by corals, calcareous red algae, and occasionally encrusting foraminifers (i.e., Acervulinidae) (see Pomar et al. 2017; Gumati 1992; Plaziat and Perrin 1992; Eichenseer 2003; Spring and Hansen 1998; Baceta et al. 2005, 2011; Aguirre et al. 2007; Mateu-Vicens et al. 2012; Morsilli et al. 2012). During this time, shallow-water settings did not feature coral reefs but were dominated by seagrass meadows, an observation that has been connected to fact that the endosymbiotic algae genus *Symbiodinium* LaJeunesse, 2017 only afterward evolved to be able to cope with such high light intensities as they do today (Pomar and Hallock 2008; Pomar et al. 2017).

Cenozoic coral bioconstructions in the well-studied Central Tethys (roughly corresponding geographically to the modern Mediterranean) thrived under low-temperature conditions, particularly during distinct periods of the Tertiary such as the early Paleocene (Danian, 66–61.6 Ma), in the Eocene (Bartonian-Priabonian, 41.2–33.9 Ma), and the early Oligocene (early Chattian, 27.8 Ma). These periods correspond to the first two diversification events of the coral endosymbiotic algae genus *Symbiodinium*, underlining the ecological importance of the evolution of this symbiont group for coral ecology. During the Early to Middle Miocene (23–8.5 Ma), corals formed small buildups and scattered colonies in the mesophotic zone (Pomar and Hallock 2007). These authors propose that the main diversification of *Symbiodinium* and the changes in the structural patterns of coral bioherms coincide with significant temperature drops within a progressive cooling trend throughout the Cenozoic. This temperature decrease induced the formation of strong thermal gradients from shallow to deep-water settings, leading to the establishment of thermoclines. Below the thermocline, water temperatures became too low for these corals to thrive, causing them to migrate upward from mesophotic to euphotic, warmer settings. Since the late Tortonian, the higher temperatures and increased light availability encountered in the surface waters, enhanced photosynthesis and its associated hypercalcification. This intense carbonate production gave rise to "modern" reefs, forming high and wave-resistant edifices. However, on the other hand, this upward movement exerted environmental pressure on the holobiont that required adaptation by the symbiotic zooxanthellae. The temperatures encountered in the water column of the Red Sea today, which are much higher than elsewhere in the

modern oceans and potentially comparable to the Cenozoic water column, might have a positive effect on calcification and reef accretion, turning them into closes modern analogs to Cenozoic mesophotic coral bioherms than mesophotic occurrences elsewhere. However, there are no studies available yet providing an assessment of calcification and accretion rates of the mesophotic bioherms in the Red Sea, thus leaving this question open for future research.

To allow for comparison of the modern example presented here with Cenozoic coral bioherms consistently thriving below the wavebase, some representative examples are briefly revisited here. In the Eocene (56–33.9 Ma), coral bioherms in the pre-Pyrenees and Pyrenees in Spain (Plaziat and Perrin 1992; Eichenseer 2003; Mateu-Vicens et al. 2012) predominantly consisted of platy-domal to massive coral colonies, encrusted by the acervulid foraminifer *Solenomeris* Douvillé, 1924 and CCA, of form low-relief coral bioconstructions (2–10 m) of low coral diversity, with red-algal nodules and *Solenomeris* in a fine-grained bioclastic matrix, indicating low-light and low-energy conditions. Locally, the coral bioherms are interbedded with sediments consisting largely of mesophotic foraminifers (Nummulitidae), with some allochthonous foraminifer taxa derived from seagrass meadows, and fragments of larger benthic foraminifers (LBF) such as *Operculina* d'Orbigny, 1826, and *Discocyclina* Gümbel, 1870. Similar to the succession described here, these coral colonies are encrusted by scarce calcareous red algae and encrusting foraminifers, including victoriellids, *Fabiania* Silvestri, 1924, *Acervulina* Schultze, 1854, *Solenomeris*, and *Haddonia* Chapman, 1898. Some coral colonies are embedded in a fine-grained (wackestone to packstone) matrix with abundant red algae and flat LBF (*Heterostegina* d'Orbigny, 1826, *Operculina*, and discoidal *Nummulites* Lamarck, 1801), similar to those found here. In the same succession, the overlying Oligocene features coral colonies along the ramp profile, while no coral colonies, but seagrass meadows, were reported in shallower settings.

More recent coral bioherms from the Chattian of Apulia, Italy, also feature coral colonies forming mounds below the wave base, at the distal talus of the escarpment, and in middle ramp settings (Pomar et al. 2014). Coeval examples from the Zagros, Iran, are characterized by large coral buildups situated below the wave base, encrusted by calcareous red algae, and infilled with a fine-grained muddy matrix. This is typical for coral bioconstructions older than the Late Tortonian that are usually found in settings below the wave base in mesophotic middle ramp settings. Nevertheless, some examples also appeared on shallower platform tops above the wave base. This may have been due to low water transparency caused by terrigenous input, as observed in the Lower Miocene of Sardinia and South-Central Turkey (Bassant et al. 2004, 2005; Janson et al. 2007, 2010; Benison et al., 2009, 2010; Pomar et al., 2012). In these areas, coral bioherms extended from the base of the slope up to the platform tops, flourishing above the wave base. Yet, instead of forming continuous reefs, these coral structures appeared as isolated buildups, with high-relief edifices only becoming common after the diversification of zooxanthellae in the Late Miocene (Pomar and Hallock 2007). In the Red Sea (e.g., Gebel Abu Shaar platform, Umluj outcrops) small buildups, biostromes, and coral carpets of poritid and faviid taxa occur along the rifted margins during Burdigalian/Langhian to Early Serravallian times (Perrin et al., 1989, Perrin 2000; Pisapia et al. 2024). These coral buildups developed on the footwall edges of basement rotated blocks, laterally associated with fan delta siliciclastic and/or bioclastic deposits containing rhodoliths, mollusks, and oolites. The corals did not form frameworks but rather cluster-segment reefs with a very fine-grained skeletal matrix.

Generally, under mesophotic to oligophotic conditions, reduced irradiance lowers photosynthesis and carbon assimilation rates, although these remain sufficient to support algal growth despite limited nutrient availability (Pomar and Hallock 2008; Pomar et al. 2017). In such environments, the advantages of algal symbiosis are subtle and episodic, primarily enhancing nutrient recycling efficiency rather than producing large amounts of photosynthates, as seen in modern euphotic coral reefs (Pomar et al. 2017). Consequently, accretion rates of meso-oligophotic constructions are lower compared to those of euphotic coral systems (Pomar et al. 2017). Nevertheless, at the scale of the bathymetric model, the geomorphometric analysis performed in this study indicates that, although direct comparisons with fossil mesophotic reefs are challenging due to differences in obtaining 3D complexity data on a comparable scale, the morphology of the present mesophotic coral ecosystem suggests that sharp, complex features, frequently associated with modern active reefs, can also characterize an active mesophotic community. In fact, similar geomorphic features observed in this study have also been reported in euphotic reefs just north of the survey area (Purkis et al. 2010; Chalastani et al. 2020; Petrovic et al. 2022).

Modern mesophotic buildups thus are typically found in extremely clear, oligotrophic waters at depths greater than 30–50 m. The increased topographic complexity of the seafloor enhances the feeding competence of suspension feeders by inducing turbulence, thereby increasing the efficiency of currents carrying plankton, which serves as the primary food source for corals. In the view of interpreting fossil coral bioherms, it is important to note that the geometry of bioconstructions not necessarily allows to distinguish between euphotic and mesophotic ones because mounds and carpets that are typical for the mesophotic can also occur in euphotic lagoons. The same concepts can also be applied to a remote sensing scale in modern environments, where similar complex geomorphic features typical from euphotic

areas can also occur in the mesophotic depths. However, when there is no ecological zonation, i.e., no difference in growth form, the possibility has to be considered that a fossil coral bioherm represents a mesophotic environment. However, as demonstrated in the present study, the skeletal assemblage, namely the taxonomy of corals, the high abundance of encrusting foraminifers, and coralline algae typical for mesophotic conditions, plus the benthic foraminifer assemblages, allows to distinguish a mesophotic origin from a euphotic one.

Conclusions

The isolated carbonate platform fragment of the Al Wajh platform represents a depth trend from euphotic to upper mesophotic conditions, through shallow to deep mesophotic conditions and transition to the aphotic realm. The organismic communities reflect the photic gradient, in particular the foraminiferal assemblages, and indicate low hydrodynamic energy in the mesophotic realm. The assemblages resemble the coral bioherms described from the pre-Upper Miocene Cenozoic when corals flourished in the mesophotic rather than the euphotic zone, as the light-resistant *Symbiodinium* strains had not evolved yet. The mesophotic example described here thus is an analog for pre-Tortonian, mesophotic coral bioherms, and helps to interpret their ecology.

Acknowledgements Thanks are due to the Topic Editor Lauren Toth and two reviewers who helped to make this a contribution bridging between the biological and geological approach to MCEs. We are grateful to the Marine Enhancement and Environmental Operations teams from the Red Sea Zone (RSZ) Environmental Protection and Regeneration department at Red Sea Global for their support in operations and for granting the permit to work in their waters. This was the 1st joint research cruise between JAMSTEC and KAUST, which was initiated by Thomas Finkbeiner (KAUST) and JAMSTEC researchers who obtained funding from the Ministry of Economy, Trade and Industry (METI) of Japan under the "Support Project for Strengthening Relations with Resource-rich Countries to Secure Oil and Natural Gas Interests and Stable Supply." The cruise took place under the COVID-19 restrictions; hence, no JAMSTEC scientists were present during the Kaja-001 cruise aboard RV Thuwal. Thanks are due to the crew of the RV Thuwal for making this cruise possible during the stormy February 2022. We are grateful to the engineering team from the Coastal and Marine Resources Core Lab (CMR) of KAUST for the technical support before, during, and after the cruise. Eloise Richardson, Dominik Nommensen, and Marlena Joppien were part of the scientific team aboard the RV Thuwal. Many thanks are due to Sebastian Flotow (ZMT) for all his help with the samples. Offboard analyses were funded by KAUST baseline to Hildegard Westphal. Geomorphometric analysis and video analysis were funded by KAUST baseline research funds to Francesca Benzoni.

Funding Open Access funding enabled and organized by Projekt DEAL. Physical Sciences and Engineering Division, KAUST, Japan Agency for Marine-Earth Science and Technology.

Declarations

Conflict of interest On behalf of all authors, the corresponding author states that there is no conflict of interest.

References

Aguirre J, Baceta JI, Braga JC (2007) Recovery of marine primary producers after the Cretaceous Tertiary mass extinction: Paleocene calcareous red algae from the Iberian Peninsula. Palaeogeogr Palaeoclimatol Palaeoecol 249:393–411

Al Tawaha M, Benzoni F, Eid E, Abu Awali A (2019) The hard corals of Jordan: a field guide. The Royal Marine Conservation Society of Jordan

Alamaru A, Loya Y, Brokovich E, Yam R, Shemesh A (2009) Carbon and nitrogen utilization in two species of Red Sea corals along a depth gradient: Insights from stable isotope analysis of total organic material and lipids. Geochim Cosmochim Acta 73:5333–5342

Al-Dubai TA, Abu-Zied RH, Basaham AS (2017) Diversity and distribution of benthic foraminifera in the Al-Kharrar Lagoon, eastern Red Sea coast. Saudi Arab Micropaleontol 63(5):275–303

Anker A, Vimercati S, Barreca F, Marchese F, Chimienti G, Terraneo TI, Rodrigue M, Eweida AA, Qurban M, Duarte CM, Pieribone V, Benzoni F (2023) Mesophotic and bathyal palaemonid shrimp diversity of the Red Sea, with the establishment of two new genera and two new species. Diversity 15(10):1028. https://doi.org/10.3390/d15101028

Augustin N, van der Zwan FM, Devey CW, Brandsdóttir B (2021) 13 million years of seafloor spreading throughout the Red Sea Basin. Nat Commun 12(1):2427

Baceta JI, Pujalte V, Bernaola G (2005) Paleocene coralgal reefs of the western Pyrenean basin, northern Spain: new evidence supporting an earliest Paleogene recovery of reefal ecosystems. Palaeogeogr Palaeoclimatol Palaeoecol 224:117–143

Baceta JI, Pujalte V, Wright VP, Schmitz B (2011) Carbonate platform models, sea-level changes and extreme climatic events during the Paleocene-early Eocene greenhouse interval: a basin-platform-coastal plain transect across the southern Pyrenean basin. In: Arenas C, Pomar L, Colombo F (eds) Pre- Meeting Field Trips Guidebook, 28th IAS Meeting, vol 7. Sociedad Geológica de España. Geo-Guías, Zaragoza, pp 151–198

Bassant P, Van Buchem FSP, Strasser A, Lomando T (2004) A comparison of two early Miocene carbonate margins: the Zhujiang carbonate platform (subsurface, South China) and the Pirinç

platform (outcrop, Southern Turkey). In: Grammer M, Harris PM (eds) Integration of Outcrop and Modern Analogs in Reservoir Modeling. AAPG Mem

Bassant P, Van Buchem FSP, Strasser A, Gorur N (2005) The stratigraphic architecture and evolution of the Burdigalian carbonate-siliciclastic sedimentary systems of the Mut Basin. Turkey Sediment Geol 173:187–232. https://doi.org/10.1016/j.sedgeo.2004.01.017

Benisek MF, Betzler C, Marcano G, Mutti M (2009) Coralline-algal assemblages of a Burdigalian platform slope: implications for carbonate platform reconstruction (northern Sardinia, western Mediterranean Sea). Facies 55:375–386. https://doi.org/10.1007/BF02536947

Benisek M-F, Marcano G, Betzler C, Mutti M (2010) Facies and stratigraphic architecture of a Miocene warm-temperate to tropical Fault-block carbonate platform, Sardinia (Central Mediterranean Sea). In: Mutti M, Piller W, Betzler C (eds) Carbonate Systems during the OligoceneeMiocene Climatic Transition. Wiley-BlackwellH

Benzoni F (2022) Re-discovery of the type material of *Leptoseris fragilis* (Cnidaria, Anthozoa, Scleractinia) from the upper mesophotic in La Réunion, a taxonomic puzzle. Zootaxa 5178(6):596–600. https://doi.org/10.11646/zootaxa.5178.6.8

Berumen ML, Hoey AS, Bass WH, Bouwmeester J, Catania D, Cochran JEM et al (2013) The status of coral reef ecology research in the Red Sea. Coral Reefs 32:737–748

Berumen ML, Arrigoni R, Bouwmeester J, Terraneo TI, Benzoni F (2019) Corals of the Red Sea. In: Voolstra CR, Berumen ML (eds) Coral reefs of the red sea. Springer International Publishing, Cham

Bongaerts P, Ridgway T, Sampayo EM, Hoegh-Guldberg O (2010) Assessing the 'deep reef refugia' hypothesis: focus on Caribbean reefs. Coral Reefs 29(2):309–327

Bongaerts P, Frade PR, Hay KB, Englebert N, Latijnhouwers KR, Bak RP, Hoegh Guldberg O (2015) Deep down on a Caribbean reef: lower mesophotic depths harbor a specialized coral-endosymbiont community. Sci Rep 5(1):1–9

Bouchon C (1981) Quantitative study of the Scleractinian coral communities of a fringing reef of Reunion Island (Indian Ocean). Mar Ecol Prog Ser 4:273–288

Bracchi VA, Basso D, Marchese F, Corselli C, Savini A (2012) Coralligenous morphotypes on subhorizontal substrate: a new categorization. Cont Shelf Res 144:10–20. https://doi.org/10.1016/j.csr.2017.06.005

Bracchi VA, Purkis SJ, Marchese F, Nolan MK, Terraneo TI, Vimercati S et al (2023) Mesophotic foraminiferal-algal nodules play a role in the Red Sea carbonate budget. Commun Earth Environ 4(1):288. https://doi.org/10.1038/s43247-023-00944-w

Briggs JC, Bowen BW (2012) A realignment of marine biogeographic provinces with particular reference to fish distributions. J Biogeogr 39:12–30. https://doi.org/10.1111/J.1365-2699.2011.02613.X

Brock VE, Chamberlain TC (1968) A geological and ecological reconnaissance off western Oahu, Hawaii, principally by means of the research submersible "Asherah." Pac Sci 22(3):373–439

Brook G (1889) The Voyage of HMS Challenger. Zoology. Report on the Antipatharia collected by HMS Challenger during the years 1873–1876. The Voyage of HMS Challenger LXXX, 1–222.

Busby R (1966) Ocean Bottom Reconnaissance Off the East Coast of Andros Island, Bahamas. US Navel Oceanographic Office, Technical Report 20390, Washington DC

Chalastani VI, Manetos P, Al-Suwailem AM, Hale JA, Vijayan AP, Pagano J, Williamson I, Henshaw SD, Albaseet R, Butt F, Brainard RE, Coccossis H, Tsoukala VK, Duarte CM (2020) Reconciling tourism development and conservation outcomes through marine spatial planning for a Saudi Giga-project in the Red Sea (The Red Sea Project, Vision 2030). Front Mar Sci 7:168. https://doi.org/10.3389/fmars.2020.00168

Colin PL, Devaney M, Hills-Colinvaux L, Suchanek TH, Harrison JT (1986) Geology and biological zonation of the reef slope, 50–360 m depth, at Enewetak Atoll, Marshall Islands. Bull Mar Sci 38:111–128

Conrad O, Bechtel B, Bock M, Dietrich H, Fischer E, Gerlitz L, Wehberg J, Wichmann V, Böhner J (2015) System for automated geoscientific analyses (SAGA) v. 2.1.4. Geosci Model Dev 8:1991–2007. https://doi.org/10.5194/gmd-8-1991-2015

Darwin C (1889) The structure and distribution of coral reefs. Smith, Elder & Co., London

Delaunay A, Baby G, Fedorik J, Afifi AM, TapponnierP Dyment J (2023) Structure and morphology of the Red Sea, from the mid-ocean ridge to the ocean-continent boundary. Tectonophysics. https://doi.org/10.1016/j.tecto.2023.229728

DiBattista JD, Roberts MB, Bouwmeester J, Bowen BW, Coker DJ, Lozano-Cortés DF et al (2016) A review of contemporary patterns of endemism for shallow water reef fauna in the Red Sea. J Biogeogr 43:423–439

Dullo W-C, Montaggioni L (1998) Modern Red Sea coral reefs: a review of their morphologies and zonation. In: Purser BH, Bosence DWJ (eds) Sedimentation and Tectonics in Rift Basins: Red Sea-Gulf of Aden: London. Chapman and Hall, pp 583–594

Dullo WC, Moussavian E, Brachert TC (1990) The foralgal crust facies of the deeper fore reefs in the Red Sea: a deep diving survey by submersible. Geobios 23:261–281

Eichenseer H (2003) Stratigraphic styles influenced by thrust tectonics: architecture and facies of lowstand wdges and transgressive to highstand carbonate banks (upper Paleocene to lower Eocene, central-southern Pyrenees). Geological Field Trip 4. In: AAPG International Conference and Exhibition 2003. Barcelona, Spain, 77 p

Einbinder S, Mass T, Brokovich E, Dubinsky Z, Erez J, Tchernov D (2009) Changes in morphology and diet of the coral *Stylophora pistillata* along a depth gradient. Mar Ecol Prog Ser 381:167–174

Eyal G, Pinheiro HT (2020) Mesophotic ecosystems: the link between Shallow and Deep-Sea habitats. Diversity 12(11):411. https://doi.org/10.3390/d12110411

Eyal G, Tamir R, Kramer N, Eyal-Shaham L, Loya Y (2019) The Red Sea: Israel. Coral Reefs of the World 12:199–214

Felis T, Lohmann G, Kuhnert H, Lorenz SJ, Scholz D, Pätzold J, Al-Rousan SA, Al-Moghrabi SM (2004) Increased seasonality in Middle East temperatures during the last interglacial period. Nature 429:164–168

Fricke H (1996) Deep-water exploration of the Red Sea by submersible. In: Uiblein F, Ott J, Stachowitsch M (eds) Deep-sea and extreme and shallow-water habitats: affinities and adaptations, Biosystematics and Ecology Series 11. Österreichische Akademie der Wissenschaften, Wien, pp 67–89

Fricke H, Hottinger L (1983) Coral bioherms below the euphotic zone in the Red Sea. Mar Ecol Prog Ser 11:113–117

Fricke HW, Knauer B (1986) Diversity and spatial pattern of coral communities in the Red Sea upper twilight zone. Oecologia 71:29–37

Fricke HW, Meischner D (1985) Depth limits of Bermudan scleractinian corals: a submersible survey. Mar Biol 88:175–187

Fricke HW, Schuhmacher H (1983) The depth limits of Red Sea stony corals: an ecophysiological problem (a deep diving survey by submersible). Mar Ecol 4(2):163–194

Fricke HW, Vareschi E, Schlichter D (1987) Photoecology of the coral *Leptoseris fragilis* in the Red Sea twilight zone (an experimental study by submersible). Oecologia 73(3):371–381

Goreau TF, Goreau NI (1973) The ecology of Jamaican coral reefs. II. Geomorphology, zonation, and sedimentary phases. Bull Mar Sci 23:400–464
Gray JE (1857) Description of a new genus of Gorgonidae. Proc Zool Soc Lond 1857:128–129
Gumati YD (1992) Lithostratigraphy of oil-bearing tertiary bioherms in the Sirte basin. Libya J Petrol Geol 15:305–318
Heaton RC, Jackson MPA, Bamahmoud M, Nani ASO (1995) Superposed Neogene extension, contraction, and salt canopy emplacement in the Yemeni Red Sea. In: Jackson MPA, Roberts DG, Snelson S (eds) Salt Tectonics: A Global Perspective. AAPG
Hillmer G, Scholz J, Dullo W-C (1996) Two types of bryozoan nodules from the Gulf of Aqaba, Red Sea. In: Gordon DP, Smith AM, Grant-Mackie JA (eds) Bryozoans in Space and Time. NIWA, Wellington National Institute of Water and Atmospheric Research
Hinderstein LM, Marr JCA, Martinez FA, Dowgiallo MJ, Puglise KA, Pyle RL, Zawada DG et al (2010) Theme section on "Mesophotic coral ecosystems: characetrization, ecology, and management." Coral Reefs 29:247–251
Hottinger L (1983) Neritic Macroid Genesis, an Ecological Approach. Coated Grains. Springer, Heidelberg, pp 38–55
Hottinger L, Hottinger L, Halicz E, Reiss Z (1993) Recent foraminiferida from the Gulf of Aqaba, Red Sea. Slovenska akademija znanosti in umetnosti 3:230
Hughes GW, Johnson RS (2005) Lithostratigraphy of the Red Sea: Geoarabia 10(3):49–126
Janson X, Eberli G, Bonnaffe F, Gaumet F, De Casanove V (2007) Seismic expression of a Miocene prograding carbonate margin, Mut Basin. Turkey AAPG Bull 91:685–713
Janson X, Van Buchem FSP, Dromart G, Eichenseer HT, Dellamonica X, Boichard R, Bonnaffe F, Eberli G (2010) Architecture and facies differentiation within a middle Miocene carbonate platform, Ermenek, Mut basin, southern Turkey. In: Van Buchem FSP, Gerdes KD, Esteban M (eds) Mesozoic and Cenozoic Carbonate Systems of the Mediterranean and the Middle East: stratigraphic and diagenetic reference models. Geol Soc London Spec Publ
Jasiewicz J, Stepinski TF (2013) Geomorphons — a pattern recognition approach to classification and mapping of landforms. Geomorphology 182:147–156. https://doi.org/10.1016/j.geomorph.2012.11.005
Kahng SE, Copus JM, Wagner D (2014) Recent advances in the ecology of mesophotic coral ecosystems (MCEs). Curr Opin Environ Sustain 7:72–81. https://doi.org/10.1016/j.cosust.2013.11.019
Kahng S, Copus JM, Wagner D (2017) Mesophotic coral ecosystems. In: Rossi S, Bramanti L, Gori A, Orejas C (eds) Marine animal forests. Springer, Cham
Kaiser P, Schlichter D, Fricke HW (1993) Influence of light on algal symbionts of the deep water coral *Leptoseris fragilis*. Mar Biol 117(1):45–52
Kendall MS, Miller T (2008) The influence of thematic and spatial resolution on maps of a coral reef ecosystem. Mar Geodesy 31(2):75–102. https://doi.org/10.1080/01490410802053617
Kühlmann DHH (1970) Die Korallenriffe Kubas. I. genese und evolution. Int Rev der Gesamten Hydrobiol und Hydrogr 55:729–756
Kükenthal W (1908) Diagnosen neuer Gorgoniden aus der Familie Plexauridae. Zool Anz 32(17):495–504
Lesser MP, Slattery M, Leichter JJ (2009) Ecology of mesophotic coral reefs. J Exp Mar Biol Ecol 375(1–2):1–8
Littler MM, Littler DS, Blair SM, Norris JN (1985) Deepest known plant life discovered on an uncharted seamount. Science 227:57–59
Littler MM, Littler DS, Blair SM, Norris JN (1986) Deep-water plant communities from an uncharted seamount off San Salvador Island, Bahamas: distribution, abundance, and primary productivity. Deep Sea Res 33:881–892
Loya Y, Eyal G, Treibitz T, Lesser MP, Appeldoorn R (2016) Theme section on mesophotic coral ecosystems: advances in knowledge and future perspectives. Coral Reefs 35(1):1–9. https://doi.org/10.1007/s00338-016-1410-7
Maggioni D, Terraneo TI, Chimienti G, Marchese F, Pica D, Cairns SD, Benzoni F (2022) The first deep-sea stylasterid (Hydrozoa, Stylasteridae) of the Red Sea. Diversity 14(4):241
Maillard C, Soliman G (1986) Hydrography of the Red Sea and exchanges with the Indian Ocean in summer. Oceanol Acta 9:249–269
Marchese F, Bracchi VA, Lisi G, Basso D, Corselli C, Savini A (2020) Assessing fine-scale distribution and volume of mediterranean algal reefs through terrain analysis of multibeam bathymetric data. A Case Study in the Southern Adriatic Continental Shelf. Water 12(1):157. https://doi.org/10.3390/w12010157
Mass T, Einbinder S, Brokovich E, Shashar N, Vago R, Erez J et al (2007) Photoacclimation of *Stylophora pistillata* to light extremes: metabolism and calcification. Mar Ecol Prog Ser 334:93–102
Mateu-Vicens G, Pomar L, Ferràndez-Cañadell C (2012) Nummulitic banks in the upper Lutetian "Buil level", Ainsa basin, South Central pyrenean zone: the impact of internal waves. Sedimentology 59:527–552. https://doi.org/10.1111/j.1365-3091.2011.01263.x
Mateu-Vicens G, Khokhlova A, Sebastian-Pastor T (2014) Epiphytic foraminiferal indices as bioindicators in Mediterranean seagrass meadows. J Foraminifer Res 44:325–339. https://doi.org/10.2113/gsjfr.44.3.325
McGarical K, Marks BJ (1995) FRAGSTATS: Spatial Pattern Analysis Program for Quantifying Landscape Structure. U.S. Department of Agriculture, Forest Service, Washington, D.C., (General Technical Report No PNW-GTR-351).
Mollenhauer G, Grotheer H, Gentz T, Bonk E, Hefter J (2021) Standard operation procedures and performance of the MICADAS radiocarbon laboratory at Alfred Wegener Institute (AWI). Ger, Nucl Instrum Methods Phys Res Sect B: Beam Interact Mater Atoms 496:45–51. https://doi.org/10.1016/j.nimb.2021.03.016
Morsilli M, Bosellini FR, Pomar L, Hallock P, Papazzoni CA, Aurell M (2012) Mesophotic coral buildups in a prodelta setting (Late Eocene, southern Pyrenees, Spain): a mixed carbonate siliciclastic system. Sedimentology 59:766–794. https://doi.org/10.1111/j.1365-3091.2011.01275.x
Muir PR, Pichon M (2019) Biodiversity of reef-building, scleractinian corals. In: Loya Y, Puglise KA, Bridge TCL (eds) Mesophotic coral ecosystems. Springer International Publishing
Nir O, Gruber DF, Einbinder S, Kark S, Tchernov D (2011) Changes in scleractinian coral Seriatopora hystrix morphology and its endocellular *Symbiodinium* characteristics along a bathymetric gradient from shallow to mesophotic reef. Coral Reefs 30:1089–1100
Opresko DM (2001) Revision of the Antipatharia (Cnidaria: Anthozoa). Part I. Establishment of a new family. Myriopathidae Zool Meded 75:343–370
Opresko DM (2002) Revision of the Antipatharia (Cnidaria: Anthozoa). Part II Schizopathidae Zool Meded 76(22):411–442
Opresko DM (2004) Revision of the Antipatharia (Cnidaria: Anthozoa). Part IV. establishment of a new family. Aphanipathidae Zool Meded 78:209–240
Orszag-Sperber F, Harwood G, Kendall AC, Purser BH (1998) A review of the evaporites of the Red Sea-Gulf of Suez rift. In: Purser BH, Bosence DWJ (eds) Sedimentation and Tectonics in Rift Basins: Red Sea-Gulf of Aden: London. Chapman and Hall, pp 409–426
Perrin C (2000) Changes of palaeozonation patterns within Miocene coral reefs, Gebel Abu shaar, Gulf of Suez. Egypt Lethaia 33:253–268

Perrin C, Plaziat JC, Rosen BR (1998) Miocene coral reefs and reef corals of the southwestern Gulf of Suez and north-western Red Sea: distribution, diversity and regional environmental controls. In: Purser BH, Bosence DWJ (eds) Sedimentation and Tectonics of Rift Basins: Red SeaeGulf of Aden. Chapman & Hall, London

Petrovic A, Fuentes M, Yahaya L, Putri I, Khanna P, Purkis S, Vahrenkamp V (2022) Holocene sediment distribution in Al Wajh platform lagoon (N Red Sea, Saudi Arabia), a modern analogue for large rift basin carbonate platforms. Sedimentology 69:1365–1398

Petrovic A, Lüdmann T, Saitz Y, Afifi AM, Betzler C, Vahrenkamp V (2023a) Fragmentation, rafting, and drowning of a carbonate platform margin. Geology 51:242–246

Petrovic A, Panara Y, Vahrenkamp V (2023) Morphological evidence of the extension of the Zabargad transform fault zone to the Saudi Arabian Red Sea margin. Geol Soc London 180(5):jgs2023-009

Petrovic A, Reijmer JJG, Alsaihati H, Nommensen D, Vahrenkamp V (2023c) Sediment dynamics and geomorphology of a submarine carbonate platform canyon system situated in an arid climate setting. Sedimentology 70(7):2241–2271

Pisapia C, Mateu-Vicens G, Benzoni F, Westphal H (2024) Mediterranean imprint on coral diversity in the incipient Red Sea (Burdigalian, Saudi Arabia). Palaios, 39, in press. https://doi.org/10.2110/palo.2023.025

Plaziat JC, Perrin C (1992) Multikilometer-sized reefs built by foraminifera (Solenomeris) from the early Eocene of the Pyrenean domain (S. France, N. Spain): paleoecologic relations with coral reefs. Palaeogeogr Palaeoclimatol Palaeoecol 96:195–231

Pomar L, Hallock P (2007) Changes in coral-reef structure through the Miocene in the Mediterranean: adaptative vs. environmental influence. Geology 35:899–902. https://doi.org/10.1130/G24034A.1

Pomar L, Hallock P (2008) Carbonate factories: a conundrum in sedimentary geology. Earth-Sci Rev 87(3–4):134–169. https://doi.org/10.1016/j.earscirev.2007.12.002

Pomar L, Bassant P, Brandano M, Ruchonnet C, Janson X (2012) Impact of carbonate producing biotas on platform architecture: insights from Miocene examples of the Mediterranean region. Earth-Sci Rev 113:186–211. https://doi.org/10.1016/j.earscirev.2012.03.007

Pomar L, Mateu-Vicens G, Morsilli M, Brandano M (2014) Carbonate ramp evolution during the late oligocene (Chattian), Salento Peninsula, Southern Italy. Palaeogeogr., Palaeoclimatol. Palaeoecol 404:109–132. https://doi.org/10.1016/j.palaeo.2014.03.023

Pomar L, Baceta JI, Hallock P, Mateu-Vicens G, Basso D (2017) Reef building and carbonate production modes in the west-central Tethys during the Cenozoic. Mar Pet Geol 83:261–304

Purkis SJ, Rowlands GP, Riegl BM, Renaud PG (2010) The paradox of tropical karst morphology in the coral reefs of the arid Middle East. Geology 38(3):227–230

Purkis SJ, Ward SN, Shernisky H, Chimienti G, Sharifi A, Marchese F, Benzoni F, Rodrigue M, Raymo ME, Abdulla A (2022) Tsunamigenic potential of an incipient submarine landslide in the Tiran Straits. Geophys Res Lett. https://doi.org/10.1029/2021GL097493

Pyle RL (2019) Advanced technical diving. In: Loya Y, Puglise KA, Bridge TCL (eds) Mesophotic coral ecosystems. Springer International Publishing, Cham, pp 959–972. https://doi.org/10.1007/978-3-319-92735-0_50

Pyle RL, Copus JM (2019) Mesophotic coral ecosystems: Introduction and overview. In: Loya Y, Puglise KA, Bridge TCL (eds) Mesophotic coral ecosystems. Springer International Publishing, Cham, pp 3–27. https://doi.org/10.1007/978-3-319-92735-0_1

Reolid J, Bialik OM, Lindhorst S, Eisermann JO, Petrovic A, Betzler C (2024) Anatomy and development of a new type of mesophotic Halimeda bioherm (Queensland Plateau, Australia). Coral Reefs. https://doi.org/10.1007/s00338-024-02500-0

Rooney J, Donham E, Montgomery A, Spalding H, Parrish F, Boland R, Vetter O (2010) Mesophotic coral ecosystems in the Hawaiian Archipelago. Coral Reefs 29(2):361–367

Rouzé H, Galand PE, Medina M, Bongaerts P, Pichon M, Pérez-Rosales G, Hédouin L (2021) Symbiotic associations of the deepest recorded photosynthetic scleractinian coral (172 m depth). ISME J 15(5):1564–1568

Rowan MG (2014) Passive-margin salt basins: hyperextension, evaporite deposition, and salt tectonics. Basin Res 26(1):154–182. https://doi.org/10.1111/bre.12043

Schlager W, Purkis SJ (2015) Reticulate reef patterns - antecedent karst versus self-organization. Sedimentology 62:501–515

Schlichter D, Fricke HW (1991) Mechanisms of amplification of photosynthetically active radiation in the symbiotic deep-water coral *Leptoseris fragilis*. Hydrobiologia 216–217(1):389–394. https://doi.org/10.1007/BF00026491

Schlichter D, Weber WT, Fricke HW (1985) A chromatophore system in the hermatypic, deep-water coral *Leptoseris fragilis* (Anthozoa: Hexacorallia). Mar Biol 89(2):143–147. https://doi.org/10.1007/BF00392885

Schlichter D, Fricke HW, Weber W (1986) Light harvesting by wavelength transformation in a symbiotic coral of the Red Sea twilight zone. Mar Biol 91(3):403–407. https://doi.org/10.1007/BF00428634

Schlichter D, Fricke HW, Weber W (1988) Evidence for par-enhancement by reflection, scattering and fluorescence in the symbiotic deep-water coral *Leptoseris fragilis* (par= photosynthetically active radiation). Endocytobiosis Cell Res 5(1):83–94

Schlichter D, Meier U, Fricke HW (1994) Improvement of photosynthesis in zooxanthellate corals by autofluorescent chromatophores. Oecologia 99(1):124–131. https://doi.org/10.1007/BF00317092

Schlichter D, Kampmann H, Conrady S (1997) Trophic potential and photoecology of endolithic algae living within coral skeletons. Mar Ecol 18(4):299–317. https://doi.org/10.1111/j.1439-0485.1997.tb00444.x

Scholz J, Hillmer G (1995) Reef-bryozoans and bryozoan-microreefs: control factor evidence from the philippines and other regions. Facies 32:109–143

Sheppard C (1982) Coral populations on reef slopes and their major controls. Mar Ecol Prog Ser 7:83–115

Shoham E, Benayahu Y (2017) Higher species richness of octocorals in the upper mesophotic zone in Eilat (Gulf of Aqaba) compared to shallower reef zones. Coral Reefs 36:71–81

Siddall M, Smeed DA, Hemleben C, Rohling EJ, Schmelzer I, Peltier WR (2004) Understanding the Red Sea response to sea level. Earth Planet Sci Lett 225:421–434

Slattery M, Lesser MP, Brazeau D, Stokes MD, Leichter JJ (2011) Connectivity and stability of mesophotic coral reefs. J Exp Mar Biol Ecol 408(1–2):32–41

Slattery M, Lesser MP, Rocha LA, Spalding HL, Smith TB (2024) Function and stability of mesophotic coral reefs. Trends Ecol Evol. https://doi.org/10.1016/j.tree.2024.01.011

Smith JE, Santamarina JC (2022) Red Sea evaporites: Formation, creep and dissolution. Earth-Sci Rev 232:104115

Sofianos SS, Johns WE (2015) Water mass formation, overturning circulation, and the exchange of the Red Sea with the adjacent basins. In: Rasul NMA, Stewart ICF, Nawab ZA (eds) The Red Sea – The Formation, Morphology, Oceanography and Environment of a Young Ocean Basin. Springer, Heidelberg, pp 343–353

Spring D, Hansen O (1998) The influence of platform morphology and sea level on the development of a carbonate sequence: the Harash Formation, Eastern Sirt Basin. Libya Geol Soc Lond Spec Publ 132:335–353. https://doi.org/10.1144/GSL.SP.1998.132.01.19

Stambler N, Levy O, Vaki L (2008) Photosynthesis and respiration of hermatypic zooxanthellate Red Sea corals from 5–75-m depth. Isr J Plant Sci 56:45–53

Strasburg DW, Jones EC, Iverson RTB (1968) Use of a small submarine for biological and oceanographic research. ICES J Mar Sci 31(3):410–426

Stuiver M, Reimer PJ (1993) Extended ^{14}C data base and revised CALIB 3.0 ^{14}C age program. Radiocarbon 35:215–230. https://doi.org/10.1017/S0033822200013904

Tapponnier P, Dyment J, Zinger MA, Franken D 2013 Revisiting seafloor-spreading in the Red Sea: Basement nature, transforms and ocean-continent boundary: American Geophysical Union Annual Fall Meeting, San Francisco, Abstract #T12B-04

Terraneo TI, Arrigoni R, Marchese F, Chimienti G, Eweida AA, Rodrigue M, Benzoni F (2022) The complete mitochondrial genome of Dendrophyllia minuscula (Cnidaria: Scleractinia) from the NEOM region of the Northern Red Sea. Mitochondrial DNA Part B 7(5):848–850

Terraneo TI, Ouhssain M, Castano CB, Aranda M, Hume BCC, Marchese F, Vimercati S, Chimienti G, Eweida AA, Voolstra CR, Jones BH, Purkis SJ, Rodrigue M, Benzoni F (2023) From the shallow to the mesophotic: a characterization of Symbiodiniaceae diversity in the Red Sea NEOM region. Front Mar Sci, Sect Coral Reef Res,. https://doi.org/10.3389/fmars.2023.1077805

Thresher RE, Colin PL (1986) Trophic structure, diversity and abundance of fishes of the deep reef (30–300 m) at Enewetak, Marshall Islands. Bull Mar Sci 38:253–272

Veron JEN (2000) Corals of the world. Australian Institute of Marine Science, Townsville

Vicario S, Terraneo T I, Chimienti G, Maggioni D, Marchese F, Purkis S J, Eweida A A, Rodrigue M, Benzoni F (2024) Molecular diversity of black corals from the Saudi Arabian Red Sea: a first assessment. Invertebrate Syst. https://doi.org/10.1071/IS23041

Vicario S, Terraneo TI, Bocanegra Castano C, Chimienti G, Oury N, Vimercati S et al (2024b) Lost in the dark: antipatharia-symbiodiniaceae association in the deep waters of the Red Sea. Front Mar Sci 11:1330118. https://doi.org/10.3389/fmars.2024.1330118

Video Lan (2006). VLC media player. Retrieved from https://www.videolan.org/vlc/index.html

Vimercati S, van der Meij SE, Terraneo TI, Chimienti G, Marchese F, Eweida AA, Benzoni F (2023) A Red Sea depth record of the coral-dwelling crab opecarcinus (Decapoda: Cryptochiridae) in the Mesophotic Zone. Diversity 15(6):723

Vimercati S, Terraneo TI, Castano CB, Barreca F, Hume BC, Marchese F et al (2024a) Consistent Symbiodiniaceae community assemblage in a mesophotic-specialist coral along the Saudi Arabian Red Sea. Front Mar Sci 11:1264175. https://doi.org/10.3389/fmars.2024.1264175

Vimercati S, Terraneo TI, Marchese F, Eweida AA, Rodrigue M, Pieribone V et al (2024b) Diversity and distribution of coral gall crabs associated with Red Sea mesophotic corals. Front Mar Sci 11:1305396. https://doi.org/10.3389/fmars.2024.1305396

Watts MAE (2022) benthic habitat mapping of thuwal's reefs using high-resolution acoustic technologies and imaging data. KAUST Res Repos. https://doi.org/10.25781/KAUST-61418

Weinstein DK, Tamir R, Kramer N, Eyal G, Berenshtein I, Shaked Y, Torfstein A (2021) Mesophotic reef geomorphology categorization, habitat identification, and relationships with surface cover and terrace formation in the Gulf of Aqaba. Geomorphology 379:107548

Wu Q, Lane CR, Wang L, Vanderhoof MK, Christensen JR, Liu H (2019) Efficient delineation of nested depression hierarchy in digital elevation models for hydrological analysis using level-set method. J Am Water Resour Assoc 55:354–368. https://doi.org/10.1111/1752-1688.12689

Xi H, Dong X, Chirayath V, Gleason AC, Purkis SJ (2024) Emergent coral reef patterning via spatial self-organization. Coral Reefs. https://doi.org/10.1007/s00338-024-02603-8

Yao F, Hoteit I, Pratt LJ, Bower AS, Zhai P, Köhl A, Gopalakrishnan G (2014) Seasonal overturning circulation in the Red Sea: 1. Model validation and summer circulation. J Geophys l Res Oceans 119:2238–2262

Zhai P, Bower AS, Smethie WM, Pratt LJ (2015) Formation and spreading of Red Sea outflow water in the Red Sea. J Geophys Res Oceans 120:6542–6563

Ziegler M, Roder CM, Büchel C, Voolstra CR (2015) Mesophotic coral depth acclimatization is a function of host-specific symbiont physiology. Front Mar Sci 2:4